# Harnessing icIEF to Unlock Protein-Based Therapeutics

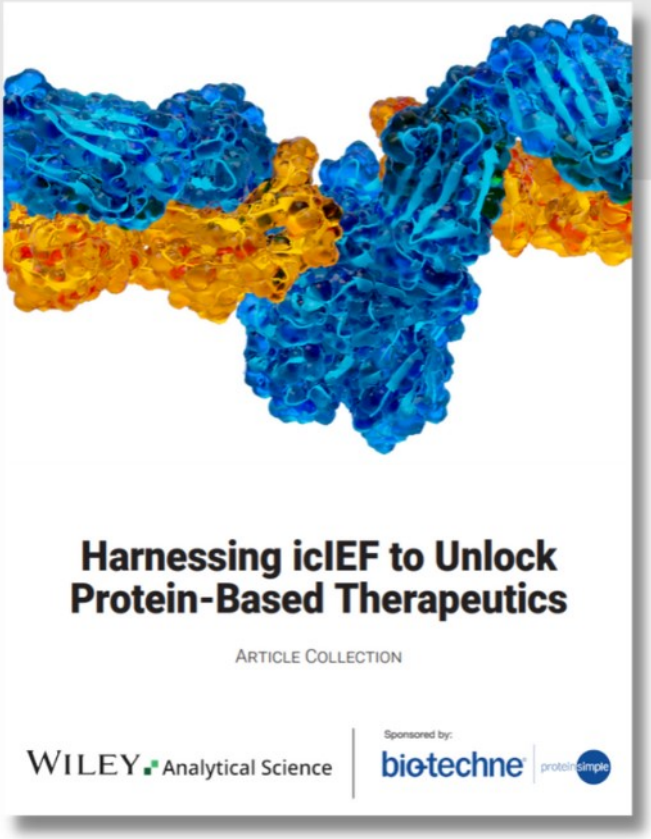


## Read the new Article Collection

Keep up to date with the latest developments in biotherapeutics and the range of treatments for various diseases with our latest article collection. Find out how imaged cIEF (icIEF) technique is essential for quality control and analytical development of these drugs, as it accurately determines the surface charge of lipid nanoparticles and the charge heterogeneity of proteins and antibodies.

This article collection aims to provide you with more information on these techniques and technologies, helping you further your research in this field.

bio-techne® | protein simple

WILEY

ADVANCED HEALTHCARE MATERIALS
www.advhealthmat.de

# Utilization of an Artery-on-a-Chip to Unravel Novel Regulators and Therapeutic Targets in Vascular Diseases

*Valentina Paloschi,* Jessica Pauli, Greg Winski, Zhiyuan Wu, Zhaolong Li, Lorenzo Botti, Sandro Meucci, Pierangelo Conti, Felix Rogowitz, Nadiya Glukha, Nora Hummel, Albert Busch, Ekaterina Chernogubova, Hong Jin, Nadja Sachs, Hans-Henning Eckstein, Anne Dueck, Reinier A. Boon, Andreas R. Bausch, and Lars Maegdefessel*

**In this study, organ-on-chip technology is used to develop an in vitro model of medium-to-large size arteries, the artery-on-a-chip (AoC), with the objective to recapitulate the structure of the arterial wall and the relevant hemodynamic forces affecting luminal cells. AoCs exposed either to in vivo-like shear stress values or kept in static conditions are assessed to generate a panel of novel genes modulated by shear stress. Considering the crucial role played by shear stress alterations in carotid arteries affected by atherosclerosis (CAD) and abdominal aortic aneurysms (AAA) disease development/progression, a patient cohort of hemodynamically relevant specimens is utilized, consisting of diseased and non-diseased (internal control) vessel regions from the same patient. Genes activated by shear stress follow the same expression pattern in non-diseased segments of human vessels. Single cell RNA sequencing (scRNA-seq) enables to discriminate the unique cell subpopulations between non-diseased and diseased vessel portions, revealing an enrichment of flow activated genes in structural cells originating from non-diseased specimens. Furthermore, the AoC served as a platform for drug-testing. It reproduced the effects of a therapeutic agent (lenvatinib) previously used in preclinical AAA studies, therefore extending the understanding of its therapeutic effect through a multicellular structure.**

## 1. Introduction

The investigation of etiopathogenetic mechanisms underlying the onset of cardiovascular diseases (CVD), as well as the study of molecular processes involved in disease progression and testing of novel therapies, have all been possible thanks to the availability of a plethora of in vivo animal models available. However, the translation of discoveries across species remains challenging when considering the unique nature of the human circulatory system, due to its mechanical, biochemical, and cellular complexities. At the same time, the use of animal models in medical research must adhere to the 3R principles (replacement, reduction, refinement).[1] In this context, the need to create in vitro models capable to mimic key aspects of human physiology/pathophysiology has led to the development of organs-on-chip (OoC), which are new tools to fill the translational gap of "animal-to-human models".[2] OoC are micro-engineered in vitro models of human

V. Paloschi, J. Pauli, Z. Wu, Z. Li, N. Glukha, N. Hummel, A. Busch, N. Sachs, H.-H. Eckstein, L. Maegdefessel
Department for Vascular and Endovascular Surgery
Technical University of Munich
80333 Munich, Germany
E-mail: valentina.paloschi@tum.de
V. Paloschi, J. Pauli, A. Dueck, L. Maegdefessel
German Center for Cardiovascular Research DZHK
Partner Site Munich Heart Alliance
80336 Berlin, Germany

The ORCID identification number(s) for the author(s) of this article can be found under https://doi.org/10.1002/adhm.202302907



**DOI: 10.1002/adhm.202302907**

G. Winski, E. Chernogubova, H. Jin, L. Maegdefessel
Department of Medicine, Cardiovascular Unit
Karolinska Institute
171 77 Stockholm, Sweden
Z. Wu
Department of Vascular Surgery
Beijing Hospital
National Center of Gerontology
Institute of Geriatric Medicine
Chinese Academy of Medical Science
Beijing 10073, P. R. China
L. Botti, P. Conti
Department of Engineering and Applied Sciences
University of Bergamo
Bergamo 24129, Italy
S. Meucci
Micronit Microtechnologies
Enschede 15 7521, The Netherlands
F. Rogowitz
FLUIGENT Deutschland GmbH
07743 Jena, Germany

organs that can recapitulate the minimal functional unit of a tissue/organ and can be used as platforms for pathophysiological studies.[3] They consist of microfluidic cell culture devices containing continuously perfused chambers inhabited by living cells arranged in a dimensional organization that preserves and mimics tissue geometry.[4] In addition, the integration of patient-derived cells and the precise control of the OoC microenvironment enhance our ability to discover novel targets and to perform drug testing using these platforms.

In the present study, we have applied OoC technology to unravel novel factors contributing to two types of cardiovascular diseases: carotid artery disease (CAD) and abdominal aortic aneurysms (AAA). CAD is a common subtype of vascular disease, in which atherosclerosis leads to narrowed arterial lumens and reduced blood flow to the brain, possibly causing transient ischemic attacks (TIA) or strokes.[5] Most commonly, carotid lesions occur at the carotid bifurcation, where a complex and rapidly varying wall shear stress (WSS) distribution is present.[6–8] AAA results from pathological widening of the aortic lumen, an asymptomatic condition that can lead to rupture with poor outcomes (mortality rate >80%).[9,10] Most of AAAs develop in the infrarenal segment of the aorta, suggesting that specific hemodynamics predispose this portion of the aorta to aneurysmal expansion and rupture.[11] Although CAD and AAA are two distinct vascular diseases,[12] both are caused by pathological remodeling of the vessel wall and influenced by alterations of hemodynamic shear stresses.[13] The endothelial layer, at the interface with blood flow, plays a relevant role in the initial stage of CAD and AAA. Subsequent pathological remodeling of the medial layer populated by smooth muscle cells (SMC) leads to lesion formation and evolution into a diseased vessel wall. Features of CAD include plaque buildup within the arterial wall, disappearance of the intima layer, and increasing inflammation corresponding to disease progression.[14,15] In aneurysms, the vessel wall becomes dysfunctional due to the loss of vascular SMC and destruction of matrix elastic fibers.[16,17]

We herein present the artery on-a-chip (AoC) model that mimics the arterial wall structure and captures potential interactions between vascular endothelial cells (EC) constantly subjected to shear stress, and underlying SMC cultured on a layer of extracellular matrix. Moreover, we show how the AoC can be used as a molecular target discovery model in CVD research and how these findings translate into the human disease context. Second, we provide evidence for the possibility of utilizing the AoC as a drug testing model, in which therapeutic agents and their effect in cellular and molecular pathophysiology can be tested.

## 2. Results

### 2.1. The AoC: An In Vitro Model of the Arterial Wall

The AoC consists of a resealable glass chip containing two flow channels separated by an intermediate layer that embeds a porous culture membrane and allows for circulation of two different fluids on each side of the membrane (**Figure 1**A). The intermediate membrane layer creates an interface for co-culture. Primary aortic EC grow on a thin layer of collagen on the flat side of the membrane, whereas primary aortic SMC are cultured on a fibronectin layer on the well-side of the same membrane (Figure 1B). To assess the quality of the coculture, immunofluorescence staining was performed using anti-PECAM and anti-SM22 antibodies, which specifically mark EC and SMC attached at opposing sides of the membrane. An entire scan of the whole membrane was performed (Figure 1C; Video 1A,B, Supporting Information). Once cells are confluent, the glass chip is assembled and sealed via a chip holder, which is ultimately connected to a microfluidic pressure controller to perfuse cell-specific culture medium (MFCS-EX from Fluigent, Villejuif, France) (Figure S1A,B, Supporting Information). The AoC is then connected to a MFCS-EX pump and integrated into an incubator (Figure S1C, Supporting Information). The flow rate is monitored and mediated externally. Throughout the experiments, the AoC was perfused for 24 h with a steady flow rate of 1.2 mL $min^{-1}$ endowing a constant WSS of 10 dyne/$cm^2$ on the EC channel. A computational flow dynamic (CFD) analysis of the AoC (bottom channel, EC) was performed in order to validate the wall shear stress distribution on the EC layer (Figure 1E,F). The flowrate in the SMC channel is 10 µL $min^{-1}$ corresponding to a maximum value of 0.0021 dyne/$cm^2$ WSS, a negligible shear stress that ensures the physiological turnover of nutrients and wastes in accordance with the in vivo situation. The flow sensors of the microfluidic platform guarantee a steady flowrate. The two 2-Switch valves (Fluigent, Villejuif, France) allow the unidirectional recirculation of EC medium between the reservoirs connected to the EC channel (Figure 1D; Figure S1C, Supporting Information).

Cells were carefully collected at both sites of the membrane, and messenger RNA (mRNA) expression of a panel of marker genes was measured to confirm specific cell identities at the

A. Busch
Division of Vascular and Endovascular Surgery
Department for Visceral
Thoracic and Vascular Surgery
Medical Faculty Carl Gustav Carus and University Hospital
Technical University Dresden
01069 Dresden, Germany

A. Dueck
Institute of Pharmacology and Toxicology
Technical University of Munich
80333 Munich, Germany

R. A. Boon
Department of Physiology
Amsterdam Cardiovascular Sciences (ACS)
Amsterdam UMC
VU University Medical Center
Amsterdam 1081 HV, The Netherlands

R. A. Boon
Institute of Cardiovascular Regeneration
Center of Molecular Medicine
Goethe-University
60323 Frankfurt, Germany

R. A. Boon
German Center for Cardiovascular Research DZHK
Partner Site Frankfurt Rhine-Main
10785 Berlin, Germany

A. R. Bausch
Department of Cellular Biophysics
Technical University of Munich
80333 Munich, Germany

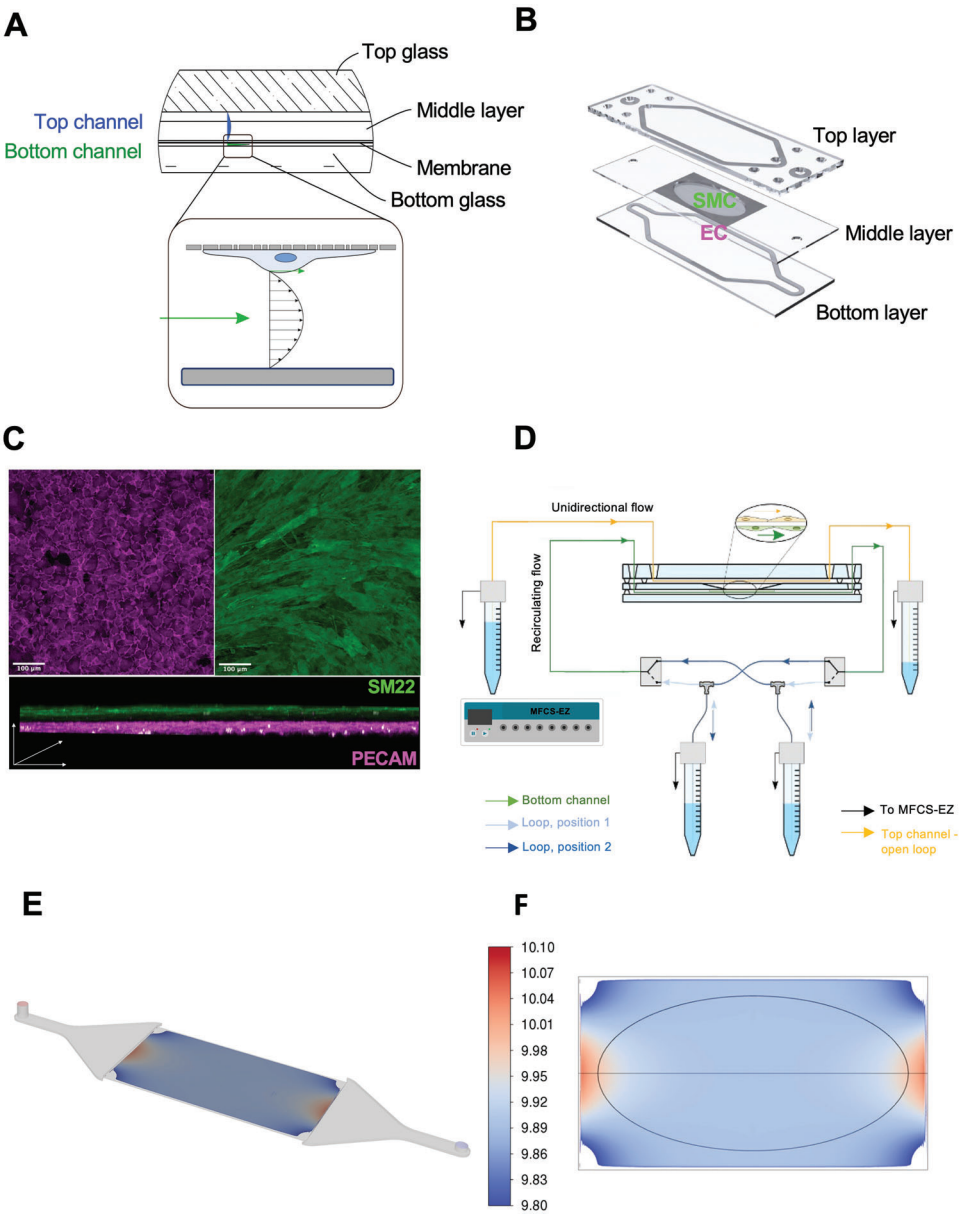


**Figure 1.** The AoC model. A) Cross-sectional design depicting the layers of the AoC and the different flow profiles in the top (blue) and bottom (green) channel, respectively. B) The membrane for co-culturing EC and SMC at opposite sides is inserted between the top and bottom layer. C) Immunofluorescence staining of the membrane shows EC and SMC, labelled by the respective cell markers (PECAM for EC and SM22 for SMC). D) Connection of the AoC to the microfluidic pump. Arrows indicate the flow direction or the connection to the pressure controller (MFCS-EZ). E,F) Computational fluid dynamic analysis (CFD) of the AoC. E) 3D view of the bottom channel (EC side) showing the location of the membrane within the AoC. The membrane region is color coded by wall shear stress (WSS). F) Detailed 2D view showing WSS distribution (ranging from 9.80 to 10.1 dyne/cm$^2$) along the membrane. The WSS threshold excludes the boundary layers located in the immediate proximity of lateral walls. EC is cultured within the ellipse.

time of cell isolation. Collagen isoforms *COL1A1*, *COL1A2*, and *COL3A1* are expressed by SMC at high levels while barely present in EC. Vice versa, von Willebrand factor (*VWF*) and *PECAM* are specifically expressed in EC, and present only at very low levels in SMC (Figure S2A,B, Supporting Information). Moreover, EC and SMC grown at opposite sides of the membrane had a similar expression pattern profile of cells growing in single culture on regular culture flask (Figure S2C,D, Supporting Information).

### 2.2. Flow-Mediated Transcriptomic Changes Identified in the AoC

RNA-seq profiles were generated from 4 AoCs exposed to flow while 4 chips were kept in static conditions. Thus, in total 16 samples (4 EC and 4 SMC for each condition) were assessed for transcriptomic changes separately within both cell types in response to flow (Tables S1 and S2, Supporting Information). Differentially expressed genes (DEGs) were identified using a statistical threshold of $P < 0.01$ and fold change of $\geq 2$ (**Figure 2**A,B;

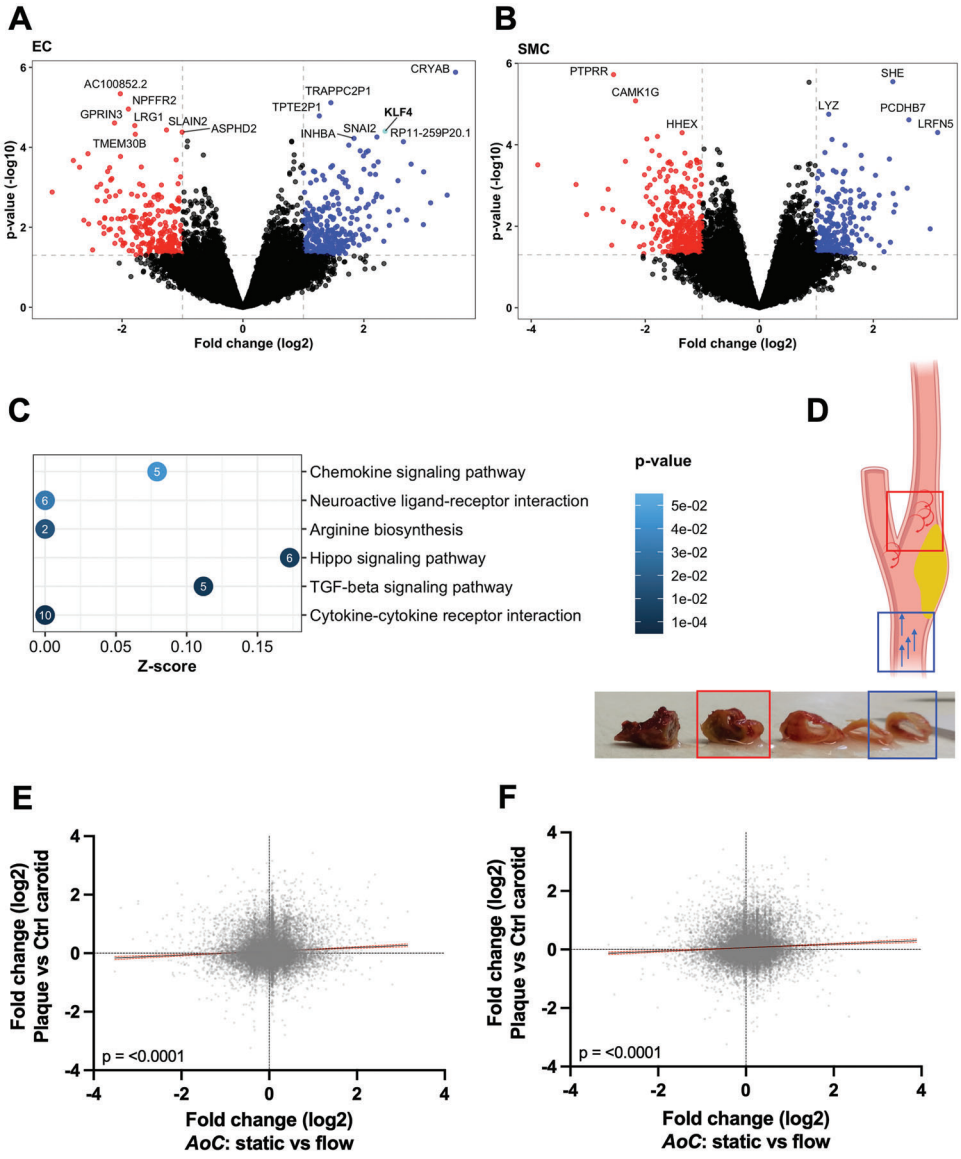


**Figure 2.** Flow-mediated transcriptomic changes identified in the AoC. Volcano plots depicting EC (A) and SMC (B), down- (red) and up- (blue) regulated mRNAs in AoCs exposed to shear versus null stress, as resulted by RNAseq experiments. Differentially expressed genes (DEGs) were identified using a statistical threshold of $P < 0.01$ with fold change $\geq 2$. At this statistical cut-off, 224 and 233 DEGs were identified in the EC and SMC contrasts respectively. The top DEGs with p-value adjusted by False Discovery Rates (FDR) corrections < 0.1 are highlighted. C) Gene-set overrepresentation analysis of KEGG pathway enrichment with enrichment Z-score on the X axis and $-\log_{10}$(p-value) on the Y axis. Point size represents pathway size and point color represents Z-score calculated as $Z = (S_u - S_d)/\sqrt{N}$, where $S_u$ and $S_d$ are the number of significant up- and down-regulated genes in the pathway respectively, and $N$ is the total number of genes in the pathway. D) Pictures of human carotid vessels with their respective schematic representations are shown. The biopsies were isolated from the most diseased location (plaque) in the vessels (indicated by red squares) and from the adjacent non-diseased area (internal control indicated by blue squares). Blue arrows show the predicted laminar flow in non-diseased areas, rotating red arrows represents the predicted turbulent flow at the diseased areas. E,F) Correlation analysis between differential gene expression in AoC static versus flow and human carotid plaques versus healthy control. Scatterplot of gene expression fold change in AoC static versus flow conditions (x-axis) and Plaque versus healthy Ctrl human carotids. All sequenced genes from the AoC experiment are shown. Black line: linear regression fit; red dashed lines: 95% confidence interval for slope. Pearson correlation p value = <0.0001 for both EC (E) and SMC (F) AoC experiments when compared with human carotid arteries.

Figure S2E,F, Supporting Information). Krüppel-like factor 4 (KLF4) and 2 (KLF2) are transcription factors previously identified as laminar flow inducible elements that play important roles in the regulation of endothelial function.[18–20] KLF4 was found upregulated in the EC of the AoC exposed to shear stress, confirming the ability of our system to replicate flow-mediated effects (highlighted in Figure 2A, Tables S3 and S4, Supporting Information). A KEGG pathway overrepresentation analysis based on the significant DEGs identified in EC in response to flow highlighted interesting, enriched pathways (Figure 2C).

Overrepresentation of DEGs that belong to "cytokine-cytokine receptor interaction" network and the "Hippo signaling pathway", whose activity strongly relies on mechanical cues in the surrounding microenvironment,[21,22] imply that EC exposed to shear stress are in an activated, stimulus-triggered state. The overrepresentation of DEGs belonging to the arginine biosynthesis pathway, precursor for the synthesis of the vasodilator nitrogen molecule nitric oxide (NO),[23] was also observed. NO is considered to be an indicator for the integrity of the endothelium.[24] Accordingly, an intact NO release can be regarded as a sign of a healthy endothelium, suggesting that a wall shear stress of 10 dyne/cm$^2$ exerts a protective effect on EC.

### 2.3. AoC-Generated Targets Are Identified in Vascular Tissues and Associated to the Non-Diseased Status

Next, we evaluated whether the findings observed in the AoC had relevance in specific portions of human vessels where disease development and progression are induced by alterations of shear stress. Thus, we assessed human tissue specimens of the Munich Vascular Biobank from patients with CAD as well as AAA.[25] From CAD patients we obtained biopsies comprising the atherosclerotic plaque (diseased artery) and the adjacent region (non-diseased artery, ctrl) (Figure 2D). Similarly, from AAA patients we obtained the aneurysmal portion (dilated aorta) and non-dilated adjacent segment (Figure S3A, Supporting Information).

At the carotid plaque site (diseased portion) the shear stress is usually low and oscillatory, while the adjacent, non-diseased portion of the vessel is likely to be subjected to unidirectional flow.[6,26] Similarly, at the aneurysmal site, shear stress alterations are likely present due to dilatation and thrombus formation.[11] There is non-laminar flow (i.e., vortex or helical flow) and resultant lower wall shears stress in the dilated aorta compared with the non-dilated upstream abdominal aorta.[27] Here, we hypothesized that the two antithetic flow conditions present in diseased and non-diseased vessels, can be matched with the two AoC models, namely the flow-exposed, constant shear stress *AoC* and the static, null shear stress AoC. We are aware that comparing the in vitro null shear stress to the hemodynamic conditions present in diseased vessels, in vivo, is over-simplified. However, given that a shear stress difference exists between a healthy vessel segment and a diseased one, we took the most differentially expressed genes by flow (identified in AoC) and measured them in human tissue specimens (Tables S1 and S2, Supporting Information).

Correlation analysis between the fold changes in DEGs observed in the AoC device and those observed in human CAD samples show that genes upregulated by flow are significantly more likely to be upregulated in the healthy segment (compared to the diseased plaque) of the human carotid arteries cohort. This result further validates our experimental setup (Figure 2E,F). The most significantly upregulated gene in EC in the AoC sequencing dataset (flow vs static) is crystallin alpha B (CRYAB), a small heat shock protein that primarily binds misfolded proteins to prevent protein aggregation, as well as inhibiting apoptosis and thus contributing to the intracellular architecture.[28] Another flow-induced gene was inhibin subunit beta A (INHBA), a member of the transforming growth factor-beta (TGF-$\beta$) superfamily of proteins. Both CRYAB and INBHA appeared significantly upregulated when comparing the non-diseased portion of the carotid vessel to the most advanced, stenotic area of the plaque within the same patient (**Figure 3**A), suggesting that shear stress-induced genes identified in the AoC might be of relevance in vivo. A reduction of elastin (*ELN*) is a prototypical signature of all diseased vessels,[29] and we sought to monitor its expression pattern in our carotid biopsies (non-disease vs stenosing atherosclerotic plaque of the same patients). As expected, there is a negative correlation between degree of disease and ELN expression (Figure 3A), highlighting the biological relevance of our cohort. Among the downregulated genes identified from the AoC after shear stress exposure (Figure 2A), leucine-rich $\alpha-2$-glycoprotein 1 (LRG1) was found significantly upregulated in the diseased portion of carotid artery (Figure 3A). Studies have demonstrated that LRG1 promotes pathogenic neovascularization and angiogenesis through activation of TGF$\beta$1 signaling pathway in EC,[30,31] and that it may also be involved in the inflammation-induced progression of atherosclerosis.[32] Moreover, LRG1 expression in EC was found to be induced by atherogenic flow and tumor necrosis factor-$\alpha$ (TNF-$\alpha$).[33] The downregulation of LRG1 strengthens the hypothesis that the applied wall shear stress has a protective effect on EC in our in vitro model. Vice versa, LGR1 upregulation in carotid diseased vessels is concordant with its detrimental role in areas likely affected by low shear stress.

Since diseased arteries are typically affected by turbulent blood flow and low shear stress, we sought to introduce another flow condition on EC. We conducted an in vitro experiment on EC introducing oscillatory flow solicitations with low shear stress (2 dyne/cm$^2$) compared to laminar flow and high shear stress (12 dyne/cm$^2$). The low shear oscillatory flow had similar effects as the null shear stress conditions applied to the AoC on the expression levels of CRYAB, LRG1, KLF2 and KLF4 (Figure 3B). This suggests that the flow response identified utilizing the AoC setup could be used to discern, within vessels, the diseased from the adjacent non-diseased portions.

In AAA specimens subjected to RNA sequencing, paired comparisons of dilated versus non-dilated aortic tissues (Figure S3A, Supporting Information) showed a trend of upregulation for both CRYAB and INHBA in the non-dilated aortic segment (Figure S3B, Supporting Information). ELN expression pattern correlated to the aneurysm onset (Figure S3B, Supporting Information). Interestingly, protocadherin beta 7 (PCDHB7), a potential calcium-dependent cell-adhesion protein with unknown function in the vasculature system, induced by shear stress in the SMC compartment of AoCs, was found to be significantly upregulated in non-dilated aortic specimens (Figure S3B, Supporting Information).

CRYAB and INHBA protein expression was evaluated via immunofluorescence in tissue sections obtained from human carotid and aortic biopsies. A loss of protein expression was observed in the diseased carotid vessel as compared to the adjacent non-diseased portion (Figures 3C and 4A). The finding was confirmed in the dilated aneurysmal aorta, as compared to the non-dilated part (Figures S3C,S4A,B,S5A, Supporting Information). CRYAB and INHBA co-localize with typical EC (VWF/PECAM) and SMC ($\alpha$SMA) markers, suggesting that the progression of both, CAD and AAA, involves EC and SMC cell populations, in which flow alterations augment the expression of

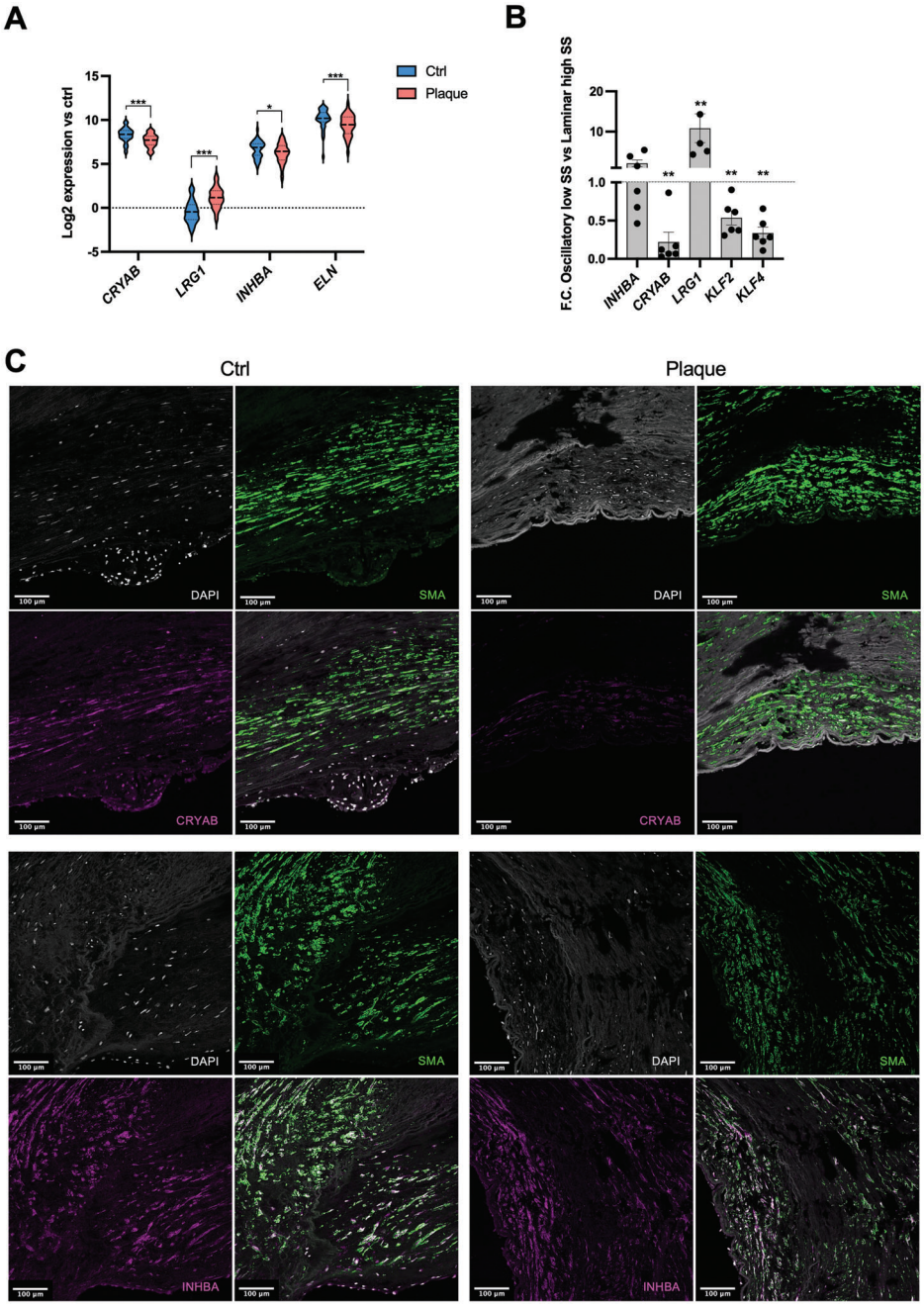


**Figure 3.** *AoC*-generated targets are identified in human vascular tissues. A) Non-diseased (Ctrl) and diseased (Plaque) carotid vessels (n = 37), as depicted in Figure 2D, were subjected to RNA-seq. ELN, CRAYB, INHBA and LRG1 expression levels are shown. Statistics: DEGs were determined by paired T-test using a statistical threshold corrected for multiple testing using the false discovery rate (FDR). (*) FDR-adjusted p-value < 0.05; (***) FDR-adjusted p-value < 0.001. B) RNA was extracted from EC exposed for 24 h to laminar high stress (12 dyne/cm$^2$) and oscillatory low shear stress (2 dyne/cm$^2$) and followed by qPCR analysis of novel flow response genes (CRYAB, INHBA, LRG1, KLF2 and KLF4). Paired T-test (n = 6) was performed. (**) p < 0.01. C) Double immunofluorescent staining of CRYAB (or INHBA) with SMA and nuclear DAPI in non-disease and diseased human carotid sections. Imaging was carried out with confocal microscopy.

responsive genes. Moreover, Western blot analyses preformed on protein lysates from non-diseased/diseased carotid arteries and non-dilated/dilated AAA human specimen reveled a significant downregulation of CRYAB and INHBA in the diseased and dilated vessels, corroborating the immunofluorescence data (**Figure 4**B; Figure S5B, Supporting Information).

### 2.4. Vascular Smooth Muscle and Endothelial Cells Are the Main Cell Cluster Expressing Flow-Induced Genes in Human Vascular Disease

Single cell RNA sequencing (scRNA-seq) was performed on human carotid plaques (Figure 4C; Figure S6A, Supporting

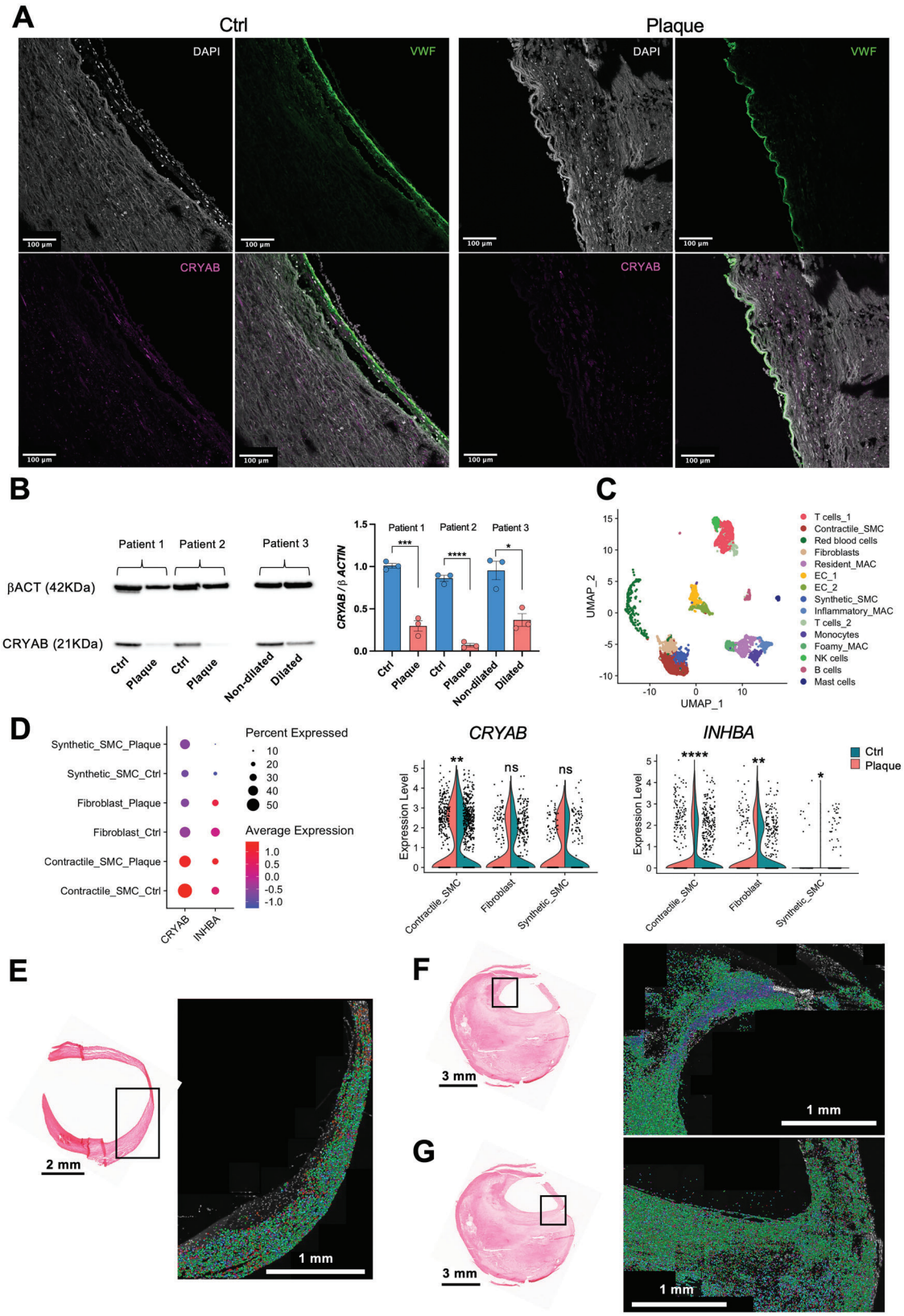


**Figure 4.** Decreased flow-induced target CRYAB in diseased carotid vessels and aortas. A) Immunofluorescence on non-disease and diseased carotid sections showing loss of CRYAB (purple) with a decrease degree of co-localization with EC marker, VWF (green) signal in diseased specimens. Imaging was carried out with confocal microscopy. B) Protein lysates extracted from non-diseased/diseased (plaque) carotid tissues (n = 2) and non-dilated/dilated

Information) and human AAA biopsies (Figure S6C, Supporting Information) on samples from the Munich Vascular Biobank. The expression levels of CRYAB and INHBA were interrogated in both datasets. In the carotid plaque scRNA-seq dataset, CRYAB and INHBA were found predominantly expressed in the fibroblast-vascular SMC (Fibro-SMC) cluster, (Figure S6B, Supporting Information). Moreover, as the non-diseased vessel (Ctrl) and diseased (Plaque) were independently prepared for individual scRNA-seq datasets from the same patients, CRYAB and INHBA expression level was compared in Fibro-SMC clusters of the two groups and found more expressed in the cell clusters of non-diseased arteries (Figure 4D). Similarly, In the AAA scRNA-seq dataset,[34] CRYAB and INHBA are enriched in structural cell clusters (Figure S6D, Supporting Information) and more highly expressed in the non-dilated SMC cluster compared to the SMC obtained from the dilated aorta (Figure S6E,F, Supporting Information).

In parallel to scRNA and bulk-seq, tissue sections of carotid plaques and control vessels were subjected to hybridization-based RNA in situ sequencing (HybRISS),[35] a probe-based targeted amplification detection method, which allows for spatial transcriptomic visualization. This approach is a validation as well as an extension of the other sequencing techniques, as it leaves the plaque architecture intact. HybRISS also enables us to identify patterns of co-expression with cell-identifying markers and therefore creates a more holistic view of disease relevance. Within an atherosclerotic plaque, the plaque shoulder region is of great importance, as it is an active area in which migrating SMC from the media layer can contribute to fibrous cap formation and confer stability or, alternatively, inflammatory processes can take place resulting in plaque progressive erosion and rupture, culminating in embolization and potential ischemic forms of stroke.[36] A control vessel and an advanced plaque[37] have been subjected to HybRISS. From a total number of 98 gene probes, we were able to detect 16.583 transcripts in the control vessel (Figure 4E), as well as 78.245 and 75.920 in two regions (shoulders) of an advanced stable carotid plaque (Figure 4F,G). In control (**Figure 5**A) CRYAB and INHBA transcripts were detected in the medial vessel layer where SMC markers (MYH11 and ACTA2) are also abundantly expressed. In the stable plaque sections (Figure 5B,C), CRYAB and INHBA transcripts were also detected in cells expressing MYH11 and ACTA2 transcripts and, to a lesser extent in von Willebrand factor (VWF)-positive cells. The expression of CRYAB and INHBA in a location where SMC stabilize the lesion[38] hints at a protective role of the identified flow response genes.

### 2.5. AoC-Identified Targets in Preclinical Experimental Vascular Disease Models

Next, we analyzed scRNA-seq data generated from mice subjected to either an inducible plaque rupture model[39] or to porcine pancreatic elastase (PPE) induced AAA formation (**Figure 6**B,G). Sham-treated mice were used as appropriate controls. Similar to the human situation of advanced vascular disease we induced an artificial flow disturbance in both preclinical mouse models. This was either provoked via ligation/obstruction of the carotid artery (Figure 6A), or by subjecting the abdominal aorta to elastase-collagenase enzyme cocktail that destroys the extracellular matrix and therefore also induces disturbed flow in the vessel (Figure 6F). Both mouse models can therefore not only be used to investigate the drivers of CAD and AAA disease, but also to investigate flow-mediated transcriptomic changes in vivo. scRNA-seq was performed separately on the treated ("diseased") and sham/non-treated ("ctrl") mice vessels, which allowed us to compare biologically relevant tissues, similarly to the approach utilized for human tissues.

In both, plaque rupture and AAA mice models, Cryab and Inhba were found to be mainly expressed by Fibro-SMC clusters (Figure 6C,H). Additionally, Cryab and Inhba expression appears significantly lower in diseased cells as compared to cells from control animals (Figure 6 D,E, I,J). On the contrary, Lrg1, a gene downregulated in the AoC exposed to shear stress and associated with the disease status of vessels, was significantly higher expressed in the EC cluster originating from murine carotid plaques/AAA tissues (Figure S7A–H, Supporting Information).

Furthermore, we obtained non-dilated and dilated portions of a large, preclinical model of AAA disease in Yucatan LDLR$^{-/-}$ mini-pigs upon local elastase instillation (Figure S7I, Supporting Information) as previously described.[40] Again, we assessed the expression level of flow-induced targets and discovered a significant decrease of INHBA in the dilated compared to the non-dilated segment accompanied by the lessening of ELN expression in all the tissue pairs (Figure S7L,M, Supporting Information).

### 2.6. CRYAB and INHBA Inhibition Affects SMC Homeostasis

To gain insights into the functional role of CRYAB and INHBA in SMC, we silenced their expression in disease-relevant human carotid SMC. The lack of CRYAB and INHBA in carotid SMC significantly altered the transcriptome profile and resulted in a great number of significant DEGs (**Figure 7**A; Figure S8A,D,G, Supporting Information). Gene Set Enrichment Analysis (GSEA) was used to associate a disease phenotype to the DEGs after CRYAB

aorta (n = 1) submitted to western blot (WB) analysis for the detection of CRYAB. Protein levels are expressed as a ratio to beta actin (bACT). Quantification of WB was done with Fiji Image J software. Statistics: unpaired T-test (*) p-value < 0.05. C) Uniform Manifold Approximation and Projection (UMAP) plot showing the major cells clusters identified from scRNA-seq performed on human carotid plaques (n = 9 patients. Ctrl and Plaque tissues are obtained from each patient). D) Dot plot and violin plot showing the higher expression and significant enrichment of CRYAB and INHBA in contractile SMC and fibroblast cell clusters originated by Ctrl as compared to Plaque specimens. The FindMarkers function was used to compare the DEGs between the Ctrl and Plaque, by using the "bimod test (Likelihood-ratio test)". (****) p<0.0001, (***) p<0.0002, (**) p<0.0021, (*) p< 0.0332. E,F,G) Ctrl (non-diseased carotid vessel) and carotid plaque were subjected to spatial transcriptomics via HybRISS methodology. All detected transcripts are shown: 16.583 transcripts in Ctrl (E), 78.245 and 75.920 in two different plaque regions respectively (F, G). The specific areas processed for spatial transcriptomic are indicated in the histochemistry images on the left side.

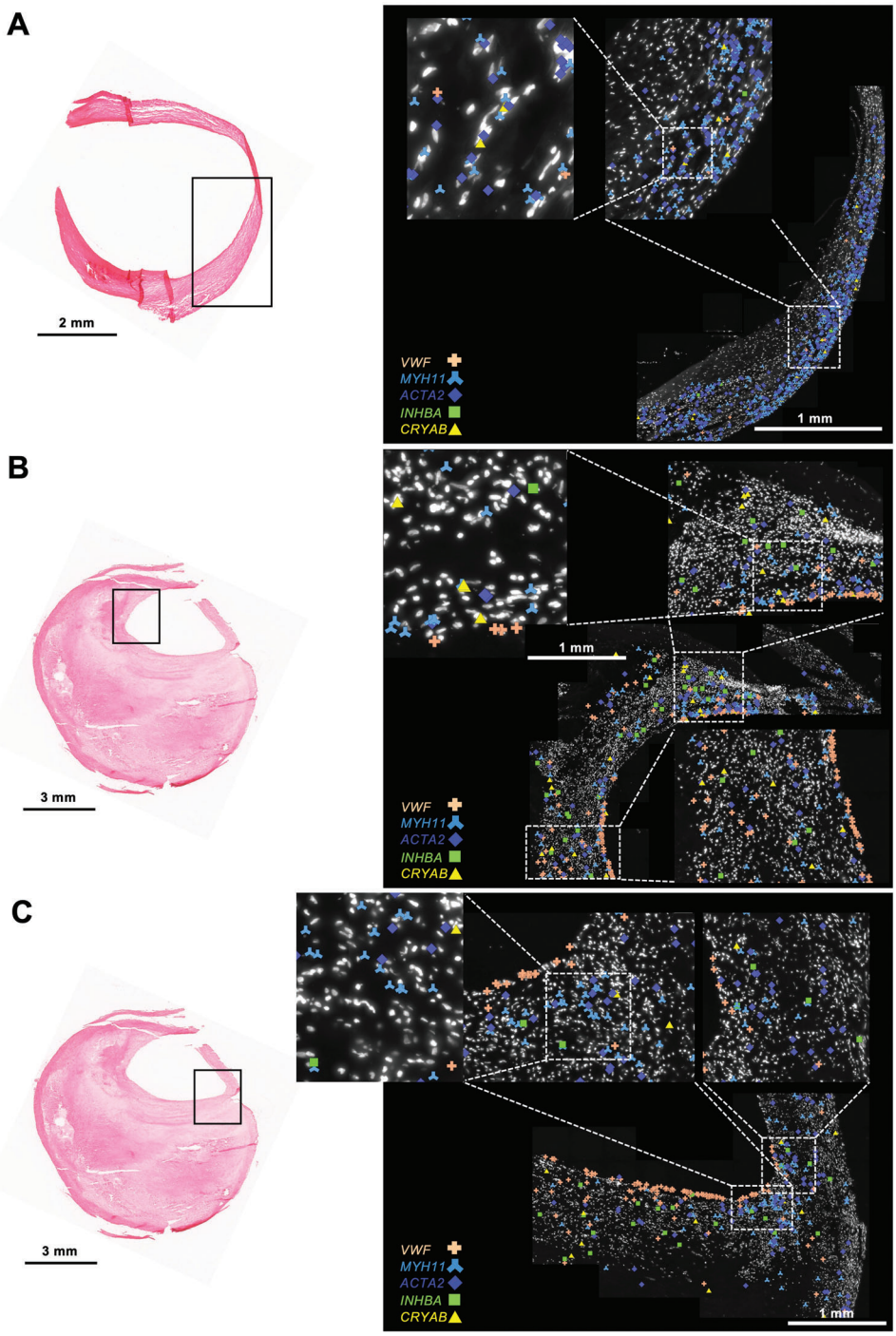


**Figure 5.** Targeted spatial transcriptomics of flow-induced targets. A) Ctrl (non-diseased carotid vessel) and B,C) carotid Plaque were subjected to HybRISS methodology. VWF, ACTA and MYH11 were chosen as prototypical markers of EC (VWF) and SMC (ACTA, MYH11) in the arterial wall. VWF, ACTA2, MYH11, INHBA, and CRYAB transcripts were detected in the tissue section and are presented in different colors. The respective processed areas are marked. In the Plaque section two different regions of the fibrous cap were analyzed.

silencing and highlighted "artery disease" and "vascular disease" as highly significant disease ontologies (Figure 7B; Figure S8B, Supporting Information). Moreover, the Human Molecular Signatures Database (MSigDB) hallmark gene sets were employed to summarize well-defined biological states or processes affected by CRYAB silencing (Figure 7C; Figure S8C, Supporting Information). The epithelial to mesenchymal transition (EMT) process is of particular interest in the context of SMC biology in atherosclerosis as EMT genes were shown to dramatically alter SMC phenotypes contributing to atherosclerotic plaque composition.[41]

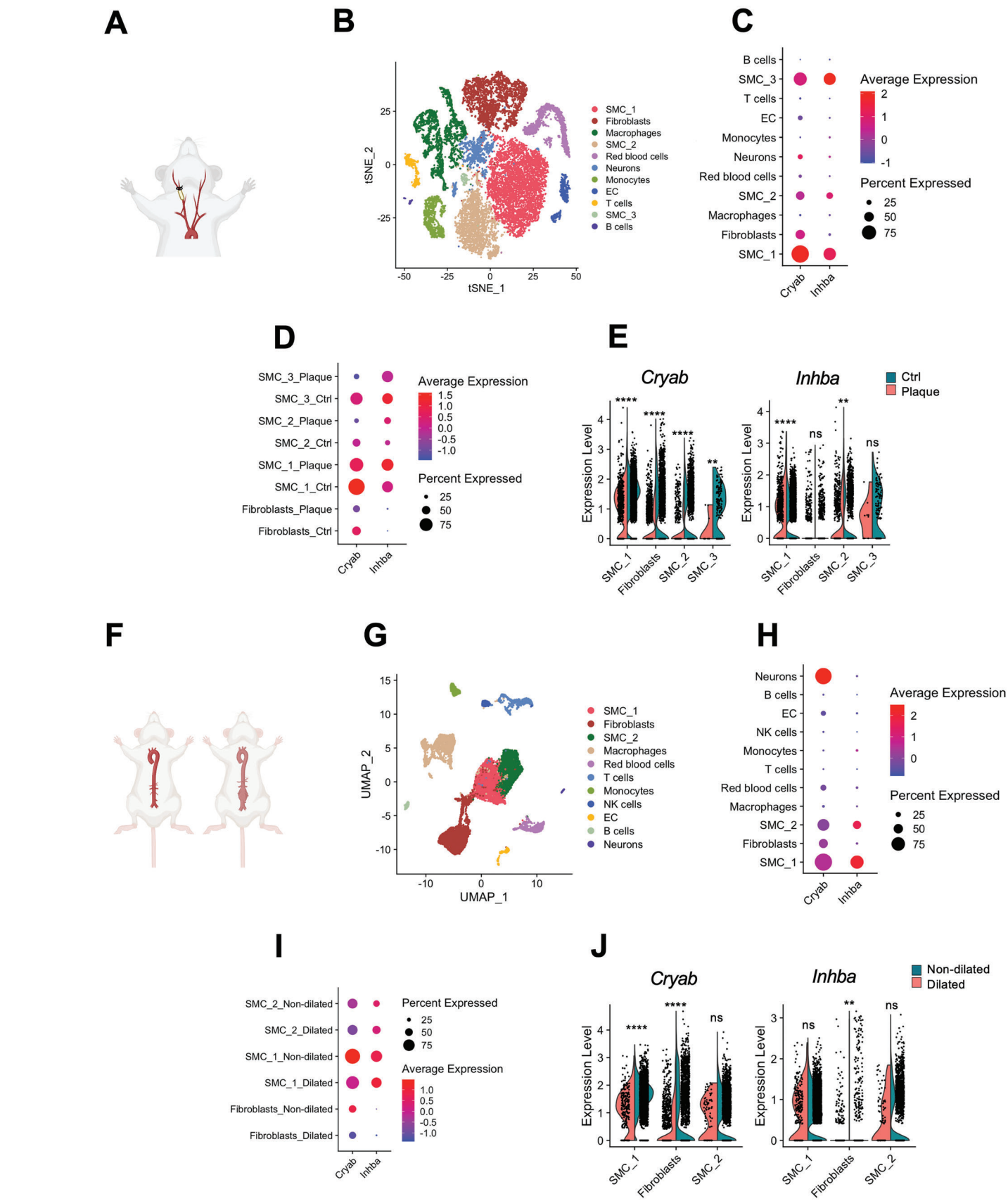

Similar results were obtained from INHBA silencing in carotid SMC with the additional enrichment of immune system disease ontology (Figure S8D–I, Supporting Information). Indeed, INHBA, a member of the TGF-$\beta$ superfamily of cytokines, plays pivotal roles in the regulation of immune responses.[42] A phenotypic analysis of the carotid SMC silenced for CRYAB or INHBA compared to control cells revealed a non-significant change in the proliferation rate, whereas a significant increase of migratory properties was detected via live cell imaging (Figure S9A,B, Supporting Information). GSEA once more indicated upregulation of EMT signaling. Altogether, CRYAB and INHBA, identified as flow response genes in our AoC, seem to have fundamental importance for the homeostasis of SMC (where they are expressed abundantly) during vascular disease development and progression.

### 2.7. AoC Serves as a Drug Testing Device for Novel Therapies in Vascular Diseases

Next, we wanted to assess whether the AoC model can serve as a drug testing device in the context of vascular diseases. This appeared possible and intriguing based on the recirculation process in the endothelial channel, mimicking the intima-blood flow interface conditions observed in vivo with possible transcellular diffusion between the cell layers.

We utilized the AoC to test the effect of lenvatinib, a tyrosine kinase inhibitor capable of limiting aortic aneurysm expansion in vivo by restoring a contractile SMC phenotype in the above-described preclinical murine and porcine models of AAA development and exacerbation[40] (Figure 7D). For these experiments, exclusively the EC layer of the AoC was exposed to circulating medium containing 10 mM of lenvatinib or DMSO (as control), whereas the SMC channel was exposed to SMC medium as described for the original AoC set up to ensure medium exchange. The SMC utilized for these experiments were isolated from patients affected by AAA to assess whether it was possible to reproduce the protective effect of lenvatinib determined in previous in vivo studies. After 24 h exposure to lenvatinib or DMSO, cells at the opposite side of the membranes were collected and the gene expression of known lenvatinib targets[40] determined. EC responded to lenvatinib with downregulation of VEGFR2 (KDR) and PECAM expression, which is consistent with its established inhibitory role in angiogenesis.[43] Moreover, lenvatinib treatment resulted in downregulation of the inflammatory activation marker VCAM1[44] (Figure 7E).

Interestingly, patient-derived SMC in co-culture with EC exposed to lenvatinib, but not directly exposed to the treatment, upregulated genes related to the contractile phenotype (ACTA2, MHY11, MYOCD) when compared to SMC co-cultured with EC exposed to DMSO (Figure 7F). This protective effect in the context of aneurysm disease recapitulated in vivo observations from our recent intervention study and is an important observation for the execution of future clinical studies in AAA patients.

## 3. Discussion

The artery-on-a-chip (AoC) mimics the architecture of the arterial vessel wall and allows to study changes induced by wall shear stress (WSS) relevant to vascular disease development and progression. WSS is the frictional force per unit area applied by the blood flow on the endothelium and it regulates important physiological blood vessel responses, such as the acute vessel tone regulation and the development of blood vessel structure during embryogenesis, as well as chronic remodeling and progression of vascular wall pathologies.[45] Imaging techniques, like phase contrast MRI, can be used to estimate blood velocity (at several locations within a given cross-sectional vessel area) and compute approximations of velocity gradients near walls.[46,47] Similarly, computational fluid dynamic analyses can be employed to predict WSS values. In a straight vessel, characterized by the Womersley-like flow behavior, vascular EC are continuously exposed to unidirectional high-shear solicitations. As a result, EC are organized in a quiescent, anti-thrombotic monolayer.[48] In contrast, flow conditions at branch points and bifurcations are often characterized by complex secondary vortices and flow instabilities resulting in low and/or oscillatory shear stresses. These solicitations promote EC proliferation and a pro-atherogenic status of the vessel wall.[49,50] Hemodynamic studies have shown that in healthy individuals the mean value of the wall shear stress (time averaged over the cardiac cycle) ranges between 8 and 10 dynes/cm$^2$ in the suprarenal aorta[51] and falls ≈8 dynes/cm$^2$ in the common carotid artery.[52] In contrast, low values of WSS are predictive of carotid plaque development[26] and correlate with AAA risk of rupture.[11] An important criterion for the development of our AoC model was the possibility to mimic shear stress of 10 dyne/cm$^2$. The imposed solicitation is different from the physiological solicitation, which is very hard to measure in vivo and to reproduce in vitro. To thoroughly replicate the shear stress solicitation in large arteries, a more complex time varying flow pattern should be provided. Nonetheless, the acquisition of patient specific flow behavior is very challenging, and even more challenging is the requirement to replicate such complex flow patterns in our AoC given the geometrical limitations of the device. Since blood flow behavior is strongly influenced by the morphology of the vessel, which is also altered by the pathology, the flow pattern is highly affected by inter-individual variability and cannot

**Figure 6.** Vascular SMC express flow-induced genes at single-cell level in mice model of CAD and AAA. A) Inducible plaque rupture mouse model: carotid vessels were isolated from control side (left) or subjected to ligation (right). B) t-distributed stochastic neighbor embedding (t-SNE) plot showing the major cells clusters identified from scRNAseq performed on mice subjected to carotid ligation. n = 9 in control and carotid plaque group (control and diseased tissues are taken from the same mouse). C) Dot plot showing Cryab and Inhba enrichment in Fibro-SMC clusters. D) Dot and E) violin plot show the higher expression and significant enrichment of Cryab and Inhba in control arteries. F) AAA mouse model (PPE infusion) and sham animals (Ctrl). G) UMAP plot showing the major cells clusters identified from scRNAseq performed on aortas isolated from control mice or subjected to the PPE-induced AAA model. In control group n = 5, and in AAA group n = 6. H) Dot plot showing Cryab and Inhba mostly expressed in the Fibro-SMC clusters. I) Dot and J) violin plot showing the significant enrichment Cryab and Inhba in Fibro-SMC clusters of control mice aortas. The FindMarkers function was used to compare the DEGs between the control and carotid plaque/AAA tissue, by using the default "Wilcoxon Rank Sum test". (****) p<0.0001, (**) p<0.0021.

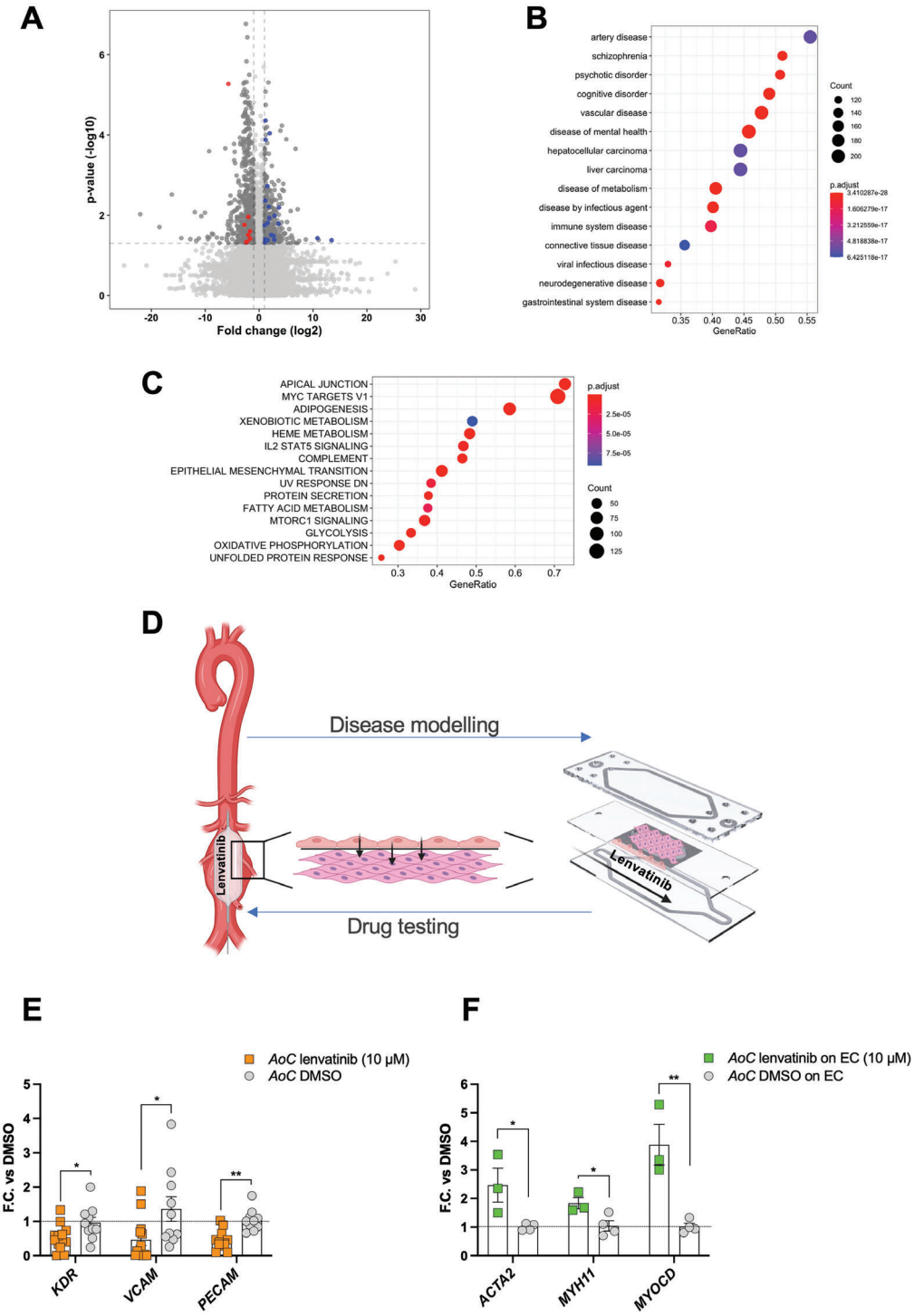


**Figure 7.** AoC as a testing model for therapeutical agent Lenvatinib. A) Volcano-plot with de-regulated genes 48 h after transfection with siCRYAB in CaSMC. Highlighted are genes contributing to GSEA score enrichment of Disease Ontology terms "Artery disease" and "Vascular disease". B,C) Gene Set Enrichment Analysis (GSEA) using Disease Ontology (B) and MSigDB Hallmark (C) gene sets. D) Scheme representing the utilization of the AoC as translational tool. Lenvatinib-coated balloon showed a therapeutical effect in halting aneurysmal progression in a pre-clinical porcine model. AAA disease modelling is partially obtained by AoC populated by AAA-derived SMC. Testing lenvatinib on the *AoC* can unravel its mechanism of action. E,F) *AoC*s exposed to lenvatinib or DMSO (ctrl) were submitted to qRT-PCR to monitor gene expression in EC and AAA-derived SMC separately. For EC analysis: DMSO group n = 10; Lenvatinib group n = 13. For AAA-derived SMC analysis: DMSO group n = 4; Lenvatinib group n = 3. Statistics: unpaired T-test (*) p-value < 0.05; (**) p-value < 0.01.

be easily standardized and brought back to a common idealized model representation. The risk of imposing unrealistic solicitations must thus be considered. For the experiments, we decided to favor reproducibility, which was a fundamental criterion for the AoC model, contemplating the pronounced variability that is inherently associated with cell co-cultures. Therefore, even if the solicitation is simplified, it has the benefit of being consistent and reproducible across all experiments.

In the present study, we tested our newly assembled AoC under shear stress (constant WSS of 10 dynes/cm$^2$) versus static condition and discovered that it can detect biologically relevant flow-inducible genes. One strength of this study relied on our human vascular biobank. The findings obtained from the AoC system were validated in specimens isolated from vascular tissues of patients affected by carotid atherosclerosis and AAA. The diseased tissue is joined by adjacent control tissue specimens. This type of analysis has not been performed before, and is likely the most suited set-up to interrogate the molecular and cellular effects of flow and shear stress alterations in human vascular disease. In vitro flow-induced expression of CRYAB and INHBA, was confirmed in non-diseased vessels obtained from patients, both at the RNA and protein level. INHBA encodes for the inhibin $\beta$A subunit of the homodimer Activin A ($\beta$A-$\beta$A), a multi-functional cytokine belonging to the TGF-$\beta$ superfamily that has been shown to inhibit vascular endothelial cell growth and angiogenesis,[53] coherently with a quiescent EC monolayer exposed to physiologically relevant shear stress. Accordingly, INHBA was found among the genes expressed by endothelial cells and their transcriptional regulation by prolonged unidirectional pulsatile flow.[54] The increased expression of CRYAB observed both in our in vitro model as well as in non-diseased human vessels could also be interpreted as protective, given its function in stabilization of cytoskeleton in response to mechanical stress.[55] These observations may support our hypothesis that the selected WSS of 10 dyne/cm$^2$ shows a vasoprotective effect on EC in vitro, with the results being translatable to human specimens. CRYAB and INHBA were indeed identified via immunofluorescence in the healthy portion of carotid arteries and aortas, and appeared to co-localize with both, EC and SMC markers.

Furthermore, the expression of CRYAB and INHBA in the vessel wall was confirmed via scRNA-seq. Fibro-SMC clusters are the mayor contributor to *CRYAB* and *INHBA* expression in both AAA and carotid data of human, with both transcripts significantly more expressed in Fibro-SMC/SMC clusters of non-diseased compared to diseased vessels. Spatial transcriptomics is a complementary method to scRNA-seq, allowing the visualization of specific transcripts in a tissue section to overcome the bias introduced by digestion protocol typical for scRNA-seq of vascular tissues.[56] This is the first time HybRISS has been performed on vascular tissue and carotid plaque sections. It allowed us to reveal that CRYAB and INHBA transcripts are found mostly in cells expressing MYH11 and ACTA2 transcripts, which again confirms SMC produce these transcripts. ScRNA-seq was also performed in preclinical murine AAA and carotid plaque rupture models, where we had the possibility to obtain also healthy aortas and carotid arteries (sham-operated animals). The comparison between the dataset originating from diseased and healthy murine vasculature showed that Cryab and Inhba are significantly higher expressed in cell clusters from control aortas and carotids. This evidence contributes to the hypothesis that flow-induced genes are present in control arteries and aortas, whereas a loss of expression is associated with the disease vessel status across different species (humans, mini-pigs, and mice). Overall, the loss of CRYAB and INHBA expression seems to have detrimental effects on the homeostasis of SMC in the arterial wall in human disease and experimental models, while being associated with vascular and immune system dysfunction.

It is intriguing to envision the AoC as a tool to perform drug testing. Any potential therapeutic agents can be transported directly to the cells via circulation, enabling us to determine the effect on the EC layer. On the other hand, the co-cultivation and intercellular communication ensured by the semi-permeable membrane offers the additional possibility to investigate the effect of the drug on the underlying SMC fraction. Administration of lenvatinib to the EC flow channel has most probably generated a signal in the EC that has been transferred to the underlying patient-derived SMC via a paracrine mechanism. By using the AoC, we provided evidence for the beneficial effect of lenvatinib in restoring SMC contractility, and gain insights into the potential mechanism of action occurring in vivo.

To the best of our knowledge, there is currently no compatible in vitro model of large sized arteries consisting of two cell layers (vascular EC and SMC) with exposure to physiologically relevant shear stress. This is due to complications relating to the lack of previous possibilities to impose high shear stress in co-culture devices. Therefore, most of the in vitro vessel models are composed of one cell type (either EC or SMC, but not co-culture) and utilize low shear stress typical of venous – but not arterial – circulation.[57] Vessel-on-chips developed to study endothelium-immune cell interaction, with the aim of gaining insights to the pathogenesis of thrombosis, consist of single channel lined with EC and perfused with blood flow but lack the integration of SMC. Recently, a microfluidic model of an artery has been reported, based on a physiologically relevant pulsatile flow behavior. However, also this system does not contain co-culture with vascular SMC.[58] Previous reports on aorta-on-chips[59,60] are composed of SMC exposed to rhythmic strain, mimicking cyclic strain due to the pulsatile nature of blood flow, but do not include EC and exposure to disease-relevant shear stress as proposed here in our model. Models that provide perfused co-culture of EC and SMC are rare,[61–63] but essential for monitoring structural changes occurring within the entire vessel wall. In our AoC model, the semi-permeable membrane between EC and SMC creates a spatial separation similar to the basal lamina, which demarcates the tunica intima from the tunica media. Second, the application of physiologically relevant shear stress resembling both the blood flow-intima interactions and the intima-media supply by diffusion, allowed us to more accurately mimic human complexity in our in vitro setup.

However, the layered structure of the vessel can only be reproduced to a limited extent by our in vitro model. For instance, EC and SMC attached to the semi-permeable membrane are aligned in a parallel fashion given the rectangular structure of the two channels. The membrane in the AoC is coated with ECM proteins (fibronectin and collagen), thus ensuring a certain interaction between ECM and cells. However, the three-dimensionality of the structure is limited by the fact that the cells and coating solutions are arranged in contiguous layers. In future developments of the

AoC model, a circumferential alignment of the SMC and the embedding it in ECM proteins would reflect a more accurate approximation of the physiological architecture of the vessel. Moreover, other physiologically relevant types of flow, such as pulsatile, oscillatory, or vorticose flow, common to the vascular branch points, could be interesting for model enhancement.

The AoC represents an original model of the arterial vessel wall by incorporating structural aspects of the vasculature (lumen-intima-media) as well as hemodynamic forces impacting the luminal cells. By increasing the capacity to emulate complex aspects of human vascular biology, the AoC could partially close the translational gap between cell culture and animal models to human pathophysiology. With the aid of this system, we were able to characterize novel targets (such as CRYAB) previously unrelated to vascular diseases as well as confirming known flow responsive genes (LRG1, INHBA, KLF2, KLF4). We were also able to demonstrate that this model system could be used as a platform for testing novel therapeutic agents and strategies in relevant (patient-derived) cell subtypes. These main characteristics demonstrate the translational potential of the AoC. In a time where the 3R criteria must be applied in experimental animal research, organs-on-chips are serving as important research tools in unravelling novel targets and therapeutic potential of drugs to human disease. The system will be of great use for future drug target discovery as well as drug testing studies in CVD research. Finally, utilization of primary patient-derived cells as well as induced pluripotent stem cells (iPSC) for evaluation of syndromic forms of vascular diseases (e.g., Marfan Syndrome or Vascular Ehlers-Danlos Syndrome) are promising areas of research for the future development of AoC.

## 4. Experimental Section

*Experimental Design: Artery-on-a-Chip*: The device utilized in this study was designed in conjunction with Micronit Technologies (Enschede, The Netherlands). It consisted of a membrane layer and two resealable glass slides that formed the top and bottom chambers for the AoC device. The standard version of the device was composed of three glass layers stacked on top of each other and compressed using a connection clamp. Two of them were the same provided in Micronit's off-the-shelf (OTS) device, the third was customized for this specific work. The standard parts were the top and bottom slides, manufactured by dispensing a fluorinated elastomer on the two 15 × 45 $mm^2$ glass parts: the first one was 0.7 mm-thick and constituted the bottom part of the chip, the second one was 1.1 mm-thick with through holes for fluidic connections and was the top part of the chip. The elastomer was processed to create a 300 µm-thick (250 µm after compression), 1 mm-wide gasket which constituted the side-walls of the chip when the stack is assembled. The chip used in this work featured a customized middle layer, made of a 0.4 mm-thick polystyrene (PS), 15 × 45 $mm^2$ in size. The slide has an elliptic hole with a 1 $cm^2$ surface (8 mm-wide, 16 mm-long) ending with a porous membrane. In this study, a commercial PET (polyethylene terephthalate) with track etched 0.45 µm-pores was used. The membrane was mounted on the middle layer using a medical grade pressure sensitive adhesive. In order to reduce the height of the bottom channel of the chip, increasing the shear stress on the bottom side of the membrane, a plateau of 100 µm was fabricated on the bottom side of the middle layer, where the membrane was mounted. As a result, the height of the bottom channel changed from the 0.2 mm of the OTS device to 0.1 mm. Instead, the height of the top chamber to the top glass channel was 0.8 mm.

Prior to cell seeding, the membrane was coated on the bottom with 0.1 mg $mL^{-1}$ collagen rat tail (Corning, USA) and on the top, where it formed a well, with 20 µg $mL^{-1}$ of fibronectin (Sigma Aldrich) to ensure cell attachment. Cells utilized on the AoC were primary human aortic endothelial cells (EC) and human aortic smooth muscle (SMC), both derived from healthy donors (Cell Application, CA, USA). Patient-derived SMC (described in the following paragraph) were also cultured on the AoC. EC and SMC were used between passages 3–7 and cultured in EC and SMC Growth Medium (PeloBiotech, Planegg, Germany), respectively. First EC were seeded on the bottom side of the membrane at a dilution of 100 000 cell/$cm^2$ and allowed to attach overnight. On the following day the membrane was flipped, and SMC was seeded (80 000 cells/$cm^2$) on the top concave side (well). On the third day, the membrane with the two distinct cell layers, was placed between top and bottom glass layers forming two separate flow chambers (Figure S1A–C, Supporting Information). The assembled AoC was secured in the chip holder, a cell culture platform, with separately controlled fluid-flows above and below. The fluid control was exerted by the connection via perfusion set to a microfluidic pressure-based pump (MFCS-EZ from Fluigent, Villejuif, France). Before the AoC connection to flow, reservoirs were filled with cell culture medium and pressurized in order to fill and rinse the tubing. To maintain the desired flow rate at a constant level along the experiment, flow sensors that monitor the flow rate were installed between the reservoirs and the AoC. A regulation algorithm was continuously evaluating the current flow rates and adjusting the pressure according to fluctuations in the flow. Flow sensors that monitor the flow rate were installed between the reservoirs and the AoC. The fluidic set up constituted by the AoC, cell culture medium reservoirs, tubing, and flow sensors were placed in a cell culture incubator (37 °C, 5% $CO_2$) and allowed to equilibrate to minimize temperature variations. The pump was placed outside the incubator and operated by MAESFLO and MAT (Microfluidic Automation Tool) software. At the end of the flow experiment (24 h after flow exposure) the AoC was disassembled, the membrane was rinsed with PBS (Gibco, Thermo Fisher Scientific) and processed for immunofluorescence staining (see paragraph below) or the harvest of EC and SMC separately. For the latter, the membrane was placed on top of a small petri dish lid with the EC facing the bottom, in contact with EC medium to prevent cells from detaching. The SMC on the concave side of the membrane, facing upward, was washed with PBS and incubated with 100 µL of 0,25% trypsin-EDTA (Gibco, Thermo Fisher Scientific) for 2 min, collected into an Eppendorf tube and centrifuged at 11 200 rpm at 4 °C for 6 min followed by pellet resuspension with 200 µL of QIAzol (Qiagen, Hilden, Germany). To isolate EC from the bottom layer, the membrane was flipped, the surface was rinsed with PBS and then scraped with 200 µL of QIAzol to collect as many cells as possible into an Eppendorf tube. Both tubes were stored at -80 °C for subsequent RNA isolation.

For immunofluorescent staining, the intermediate membrane layer populated by EC and SMC was fixed at the end point of the experiment by immersion in 4% paraformaldehyde (Thermo Fisher Scientific) for 20 min, followed by incubation in blocking buffer containing 5% bovine serum albumin (BSA, Sigma-Aldrich, St. Louis, MO, USA) in PBS. The membrane was incubated with antibodies against PECAM (ab9498, abcam) 1:20 and against SM22 (ab170902, abcam) 1:200 (in PBS containing 3% normal goat serum and 0,3% Triton-X100) for 4 h at room temperature. The appropriate secondary antibodies (Alexa647 anti mouse (A21236) and Alexa488 anti rabbit (A11034)) were added for 1 h (1:400 in PBS containing 3% normal goat serum and 0,3% Triton-X100). The incubation of primary and secondary antibodies was performed simultaneously on the membrane, with volumes touching the bottom and the upper side. Cells nuclei were stained with DAPI (Thermo Fisher Scientific) for 5 min. After the immunofluorescent staining, the membrane was first isolated from the plastic support of the intermediate layer and mounted between a glass slide and a coverslip. It was then imaged perpendicular to the objective with an Olympus FLUOVIEW FV3000 (Olympus, Tokyo, Japan) confocal microscope. A z-stack image was taken from the endothelial (bottom) to the smooth muscle (upper) layer.

*Shear Stress Calculation*: Shear stress calculation was based on the assumption of fully developed laminar flow in a duct with rectangular cross section. The rectangular cross section had large aspect ratio, in particular the width (b) was much larger that the height (2 delta), therefore, away from lateral walls, the flow can be treated as 2D. Here, we describe the

flow based on a cartesian reference frame with the y and z axis perpendicular to the bottom and lateral wall, respectively. The velocity has only axial component (u) which is a function of the y coordinate. Applying the linear momentum equation in the x direction, it is possible to infer that the velocity profile u(y) is parabolic and the pressure gradient dp/dx is linear. We are therefore dealing with Poiseuille flow.

The velocity profile can be expressed as a function of the flow and geometrical parameters, as

$$u(y) = \frac{3}{2}\frac{Q}{A}\left(1 - \frac{y^2}{\delta^2}\right) \quad (1)$$

where Q is the volumetric flow rate, $A = 2\,\delta\,b$ is the area of the rectangular cross section, and $2\,\delta$ is the channel height. The wall shear stress magnitude can be easily computed from its definition, we obtain

$$\tau_w = \frac{3\,\mu\,Q}{2\,\delta^2\,b} \quad (2)$$

where μ is the fluid viscosity. For the *AoC*: Q = 1.2 mL $min^{-1}$ ( = 0.02 $cm^3/s$), μ = 7,5 * $10^{-3}$ g $cm^{-1}$ s, $\delta$ = 0.005 cm, b = 0.9 cm.

Computational flow dynamic (CFD) analysis of the *AoC* (bottom channel, EC) was performed in order to validate the wall shear stress distribution on the EC layer. Based on a computer-aided design (CAD) model of the AoC (provided by Micronit) the commercially available Ansys fluent software (Canonsburg, USA) was employed to numerically simulate the flow behavior and wall shear stress distribution (Figure 1E,F).

Cell Culture under Flow

EC were seeded in μSlides $^{0.2}$ / μSlides $^{0.6}$ (Ibidi, Munich, Germany) and connected to the pump (Ibidi, Munich, Germany) according to the manufacturer's protocol. EC were exposed simultaneously for 24 h to either laminar flow providing a shear stress of 12 dyne/$cm^2$ or oscillatory flow with a frequency of oscillation of 2 s, providing a shear stress of 2 dyne/$cm^2$.

*Munich Vascular Biobank*: Human aortic aneurysm samples, as well as human carotid artery specimen were collected from the Munich Vascular Biobank, as described previously upon patients' informed consent.[25] The biobank was approved by the local Hospital Ethics Committee (2799/10, Ethics Committee of the Faculty for Medicine at the Technical University of Munich, Munich, Germany) and in accordance with the Declaration of Helsinki. Primary human aortic SMC from patients were isolated from AAA biopsies, harvested during surgical repair and stored in complete DMEM/F12 Medium (Sigma Aldrich) containing 5% Fetal Bovine Serum (Gibco, Thermo Fisher Scientific) and 1% Pen-Strep (Gibco, Thermo Fisher Scientific). The tissue was placed in a sterile petri dish and washed with PBS (Gibco, Thermo Fisher Scientific). Adventitia, neo-Intima and calcifications were removed, and the remaining media was cut into small pieces using a sterile scalpel. The pieces of tissue were placed in digestion medium (1.4 mg $mL^{-1}$ Collagenase A, Roche, Mannheim, Germany, in complete DMEM/F12 Medium) in a humidified incubator at 37 °C and 5% CO2 for 4–6 h. Cells were strained using a 100 μm cell strainer to remove debris. After two washing steps (centrifuge 400 g, 5 min; discard supernatant, re-suspend in 15 mL complete DMEM/F12 Medium) cells were re-suspended in 7 mL complete DMEM/F12 Medium and placed in a small cell culture flask in a humidified incubator at 37 °C and 5% CO2. Upon confluence, cells were stored in liquid nitrogen or processed immediately. SMC isolated from abdominal aortas were used between passages 3–6.

For lenvatinib experiments, the EC side was exposed to medium (Optimem only supplemented with antibiotics (1%) and 2% of FBS, containing lenvatinib 10 μM or its control (DMSO). The SMC channel was exposed to regular SMC medium.

*RNA Isolation and RT-qPCR Analysis*: Human and porcine carotid artery/aortic tissues were cut in ≈50 mg pieces on dry ice. Use of the pig tissue was approved by the Regional Government of Upper Bavaria (Oberbayern), Germany (Ethics approval number is Vet_02-18-53). Tissue was homogenized in 700 μL Qiazol lysis reagent and total RNA was isolated using the miRNeasy Mini Kit (Qiagen, The Netherlands) according to manufacturer´s protocol. EC and SMC from AoC experiments were collected as described above, and total RNA was isolated using the miRNeasy Micro Kit (Qiagen, Netherlands) according to manufacturer´s protocol. RNA concentration and purity were assessed using the NanoDrop system (Thermo Fisher Scientific). RNA Integrity Number (RIN) was assessed using the RNA Screen Tape (Agilent, USA) and the Agilent TapeStation 4200. Next, first strand cDNA synthesis was performed using the High-Capacity-RNA-to-cDNA Kit (Applied Biosystems, USA), following the manufacturer's protocol. Quantitative real-time TaqMan PCR was then performed using primers for the genes listed below:

| | |
|---|---|
| RPLPO | HS00420895_gH |
| PECAM1 | HS01065279_M1 |
| VWF | HS01109446_M1 |
| COL1A1 | HS00164004_M1 |
| COL1A2 | HS01028970_M1 |
| COL3A1 | HS00943809_M1 |
| SMTN | Hs01022255_g1 |
| KLF2 | Hs000360439_m1 |
| ELN | Hs00355783_m1 |
| INHBA | Hs01081598_m1 |
| CRYAB | Hs00157107_m1 |
| LRG1 | Hs00364835_m1 |
| KDR | Hs00911700_m1 |
| VCAM1 | HS01003372_M1 |
| ACTA2 | HS00426835_G1 |
| MYH11 | HS00975796_M1 |
| MYOCD | Hs00538076_m1 |
| INHBA | Ss03393536_s1 |
| CRYAB | Ss06921086_m1 |
| RPLP0 | Ss03389091_m1 |
| ELN | Ss04955056_m1 |

*Cell Culture and Transfection of Human Carotid Smooth Muscle Cells*: Primary human carotid smooth muscle cells (hCASMC) were obtained from PeloBiotech (#PB-3514-05a) and cultured in Smooth Muscle Cell Growth Medium (PeloBiotech, Munich, Germany), following the manufacturer's protocol. Transfection of small interference RNA (siRNA) was performed using Lipofectamine RNAiMAX (Thermo Fisher Scientific, Waltham, MA, USA) mixed with anti-CRYAB, anti-INHBA or scrambled controls (Ambion, California, USA) for a final concentration of 25 nM. Two different timepoints (48hs and 72hs) were investigated. After that, cells were harvested in 700 μL Qiazol and total RNA was isolated using the miRNeasy Micro Kit (Qiagen, Netherlands) according to manufacturer´s protocol. RNA concentration and purity were assessed using the NanoDrop system (Thermo Fisher Scientific). RNA Integrity Number (RIN) was assessed using the RNA Screen Tape (Agilent, USA) and the Agilent TapeStation 4200.

*Dynamic Live-Cell Imaging Assays*: All dynamic live-cell imaging experiments were performed following the instructions provided by Essen Bioscience (Ann Arbor, MI, USA) using the IncuCyte ZOOM system. Carotid SMC were plated in 48-well plates for proliferation assay (Corning/Falcon, Tewksbury, MA, USA) or 96-well ImageLock plates (Essen Bioscience, Ann Arbor, MI, USA) for migration assay, followed by transfection with anti-CRYAB, anti-INHBA or scrambled controls (Ambion, California, USA). Proliferation was monitored over 72 h using the IncuCyte ZOOM System. Images were auto-collected and analyzed using the IncuCyte ZOOM software (Essen Bioscience, Ann Arbor, MI, USA). Homogeneous 700–800 μm wide wounds were created using the WoundMaker (Essen Bioscience, Ann Arbor, MI, USA) 24 h after transfection. The plate was monitored in the IncuCyte ZOOM System (Essen Bioscience, Ann Arbor, MI, USA) with a 2 h

imaging pattern. Images were auto-collected and analyzed using the IncuCyte ZOOM software (Essen Bioscience, Ann Arbor, MI, USA).

*RNA Sequencing (RNAseq)*: RNA sequencing of EC and SMC exposed to shear/null stress was performed using the IonTorrent Chef System (Thermo Fisher Scientific). A total of 10 ng RNA was reverse-transcribed using Invitrogen Superscript VILO cDNA Synthesis Kit (Thermo Fisher Scientific). Transcriptome libraries were generated using automated library preparation with the Ion AmpliSeq Transcriptome Human Gene Expression Kit (Thermo Fisher Scientific). The transcriptome libraries were barcoded, templated, and sequenced on the Ion Chef and Ion GeneStudio S5 Prime systems using Ion 550 Kit-Chef and Ion 550 Chip Kit, as one 16-plex library pool. The quality of the raw expression data was evaluated by Fios Genomics (Edinburgh, UK) using several automated outlier tests. One sample (EC exposed to flow) failed two of these outlier tests and was therefore excluded from subsequent analysis. Expression data was provided as a count matrix for 55765 features in each sample. 33357 features with a maximum read count less than or equal to zero across all samples were excluded from analysis. Normalization was carried out using trimmed mean of M-values normalization and expression values were transformed using voom.

Extracted RNA from non-diseased (ctrl) and diseased (plaque) tissue biopsies obtained from 37 patients undergoing carotid endarterectomy as well as from non-dilated and dilated tissue biopsies from 7 AAA patients, was used to generate libraries that where sequenced via the Illumina NovaSeq platform. (NovaSeq6000, Illumina, San Diego, USA). RNA was purified from total RNA using poly-T oligo-attached magnetic beads. After fragmentation, the first strand cDNA was synthesized using TruSeq stranded total RNA kit and TruSeq stranded mRNA kit (Illumina, San Diego, USA), followed by the second strand cDNA synthesis using dUTP. The directional library was ready after end repair, A-tailing, adapter ligation, size selection, amplification, and purification. The library was checked with Qubit and real-time PCR for quantification and Bioanalyzer for size distribution detection. Raw data (raw reads) of FASTQ format were analyzed by Fios Genomics (Edinburgh, UK). Quality control (QC) was performed on the raw FASTQ files and the alignment statistics generated by the STAR aligner during the data processing protocol. All samples exhibited high quality and consistent sequence length distributions, so they were all included in subsequent analyses (Fios Genomics, Edinburgh, UK). RNA extracted from human carotid SMC silenced for CRAYB and INHBA (and respective controls) was subjected to sequencing the Illumina NovaSeq6000 platform at Novogene (Cambridge, UK).

*Tissue Immunofluorescence Staining*: *Carotid arteries*: 3 µm sections of formalin fixed and paraffin-embedded (FFPE) human carotid artery samples from the Munich Vascular Biobank[25] were mounted on 0.1% poly-L-lysine (Sigma-Aldrich, St. Louis, MO, USA) pre-coated SuperFrost Plus slides (Thermo Fisher Scientific, Waltham, MA, USA) and dried over night at 56 °C. Sections were dewaxed and heat mediated antigen retrieval was performed using a pressure cooker with 10 nM citrate buffer (distilled water with citric acid monohydrate, pH 6.0). Endogenous peroxidase activity was blocked with 3% hydrogen peroxide. Two antibodies were applied in sequence. For each antibody, samples were blocked for 1 h (5% horse serum, 1%BSA, 0,5% Triton-X100) and incubated with primary antibodies diluted in 5% horse serum overnight. The appropriate secondary antibody was added for 1 h (in 5% horse serum) on the next day. Autofluorescence quenching and counterstaining with DAPI were performed. Images were acquired with an Olympus FLUOVIEW FV3000 (Olympus, Tokyo, Japan) confocal microscope.

*Aortic aneurysms*: Aortic aneurysm tissue was harvested during open repair in our clinical Department for Vascular and Endovascular Surgery (Klinikum rechts der Isar) in Munich. Tissue was placed in RNAlater (Sigma-Aldrich, St. Louis, MO, USA) on ice until further processing. The tissue was cut in several pieces and the most morphologically relevant pieces were snap frozen in liquid nitrogen and immediately embedded in Tissue-Tek O.C.T. (Optimal Cutting Temperature) Compound. OCT embedded tissues were stored at -80 °C until further use. Ten µm sections of OCT embedded samples were mounted on SuperFrost Plus slides (Thermo Fisher Scientific, Waltham, MA, USA) and stored at -80 °C until further use. Sections were fixed in ice cold acetone for 5 min. Endogenous peroxidase activity was blocked with 3% hydrogen peroxide. Blocking, subsequent antibody staining, autofluorescence quenching, counterstaining with DAPI, and imaging were performed as described above for carotid artery FFPE tissues.

**Antibodies**:

CRYAB (ab13496, abcam) 1:50
INHBA (ab56057, abcam) 1:25
VWF (ab6994, abcam) 1:3000
PECAM (ab9498, abcam) 1:50
SMA (ab7817, abcam) 1:200
SMA (ab5694, abcam) 1:200
Alexa488 anti rabbit (A11034) 1:400
Alexa488 anti mouse (A11001) 1:400
Alexa647 anti rabbit (A21245) 1:400
Alexa647 anti mouse (A21236) 1:400

*Western Blot Analysis*: Fresh frozen human aortic aneurysm and carotid artery tissue were cut in ≈50 mg pieces on dry ice. Tissue was homogenized in 200 µL Tissue Extraction Reagent I (Thermo Fisher, USA). After homogenization with the Bio-Gen PRO200 Homogenizer and Multi-Gen 7XL Probes (Pro Scientific, USA), samples were centrifuged for 20 min, 14.000 rpm at 4 °C and the supernatant was frozen down at -80 °C. Total protein concentration was measured using the Pierce BCA Protein Assay Kit (Thermo Fisher) following manufacturer´s protocol. 10 µg of protein from each sample was denatured and reduced at 70 °C for 10 min, then separated in a Bolt 4–12% Bis-Tris Plus Gel (Thermo Fisher) and transferred onto Trans-Blot Turbo Mini-Size LF-PVDF Membranes (BioRad, Hercules, CA, USA). The blots were blocked with 5% milk in Tris-buffered saline+0.1% Tween-20 for 1 h, followed by overnight incubation with the primary antibody against INHBA/CRYAB/bACT in TBS-T+5%milk. After washing with TBS-T, blots were developed with horseradish peroxidase (HRP)-conjugated secondary antibody (Abcam, Cambridge, UK) for 1 h in combination with ECL (GE Healthcare, Chicago, IL, USA). Image detection was performed with C600 Azure Biosystems Imager (Biozym)/ChemiDoc XRS System (Bio-Rad, Hercules, CA, USA). Image quantification was done using ImageJ software.

**Antibodies**:

CRYAB (ab13496, abcam) 1:1000
INHBA (ab56057, abcam) 1:1000
b-ACTIN (A5316, Sigma Aldrich) 1:8000
HRP-conjugated secondary (ab205718, ab205719, abcam) 1:10 000

*Single Cell RNA Sequencing (scRNA-seq)*: *Human vessel dissociation*: Human carotid or abdominal arteries were harvested during carotid endarterectomy or open repair in our Department of Vascular and Endovascular Surgery (Klinikum rechts der Isar, TUM). The biopsies were minced and digested using the Multi Tissue Dissociation Kit 2 (Miltenyi Biotech, 130-110-203), GentleMACS Dissociator (Miltenyi Biotech, 130-093-235), GentleMACS C tubes (Miltenyi Biotech, 130-096-334) and the 37 C_Mulit_G program, all according to the manufacturer´s instructions. The cell suspension was strained (70 µm, 40 µm) and Dead Cell Removal (Miltenyi Biotech, 130-090-101) using MS Columns (Miltenyi Biotech, 130-042-201) was performed was performed. Cells were resuspended in PBS + 0,04% BSA.

*Mouse vessel dissociation*: Mouse carotid or abdominal arteries were harvested in Stockholm following approval by the Ethics Committee of Northern Stockholm, Sweden (approval number DNR6722-2021). The treated (Carotid Plaque Rupture Model n = 9 or PPE-AAA n = 6) and untreated (carotid artery n = 9 or aorta n = 5) tissues were transported in PBS on ice to the laboratory. The tissues were cut into small pieces with a surgical scissor and digested using the following enzymes: Liberase 4U $mL^{-1}$ (Sigma Aldrich, 5 401 127 001), Hyaluronidase 60 U $mL^{-1}$ (Sigma Aldrich, H3506-100MG) and DNAse 120 U $mL^{-1}$ (Thermo Fisher, 18 047 019) in RPMI Medium + 10%FBS at 37 °C with agitation for 45 min. The cell

suspension was strained (70 µm, 40 µm) and Dead Cell Removal (Miltenyi Biotech, 130-090-101) using MS Columns (Miltenyi Biotech, 130-042-201) was performed. Cells were resuspended in PBS + 0,04% BSA.

*Single-cell capture and library preparation*: Cells were loaded into a 10x Genomics microfluidics Chip G and encapsulated with barcoded oligo-dT-containing gel beads using the 10x Genomics Chromium Controller. Gel Beads-in-emulsion (GEM) cleanup, cDNA Amplification and 3´Gene Expression Library Construction was performed according to the manufacturer´s instructions (CG000204 Rev D).

*RNA sequencing*: Human: Libraries from individual samples were multiplexed into one lane before sequencing on an Illumina NovaSeq6000 instrument. Mouse: Libraries from individual samples were loaded on an Illumina NovaSeq with 2 × 150 paired-end kits at Novogene.

*ScRNA-seq analysis*: ScRNA-seq analyses were performed according to Seurat instructions (version 4.3.0) in R (version 4.0.3). Genes were excluded for downstream analysis if expressed in fewer than 5 cells. Cells would also be filtered out in each Seurat object if they fulfilled the following conditions: maximum mitochondrial reads >15%, maximum UMIs more than 20 000, minimum genes less than 100 and maximum genes more than 3 000–4 000. CellCycleScoring function in Seurat was applied to obtain the scores of cell cycle phases including S phase and G2M phase. SCTransform normalization workflow was adopted to mitigate possible technically driven or other variations, in which mitochondrial genes and cell cycle phase were regressed. T-SNE (t-Distributed Stochastic Neighbor Embedding)/UMAP (Uniform Manifold Approximation and Projection) were used to convert cells into a 2D map. FindAllMarkers function was performed to detect the main features of each cluster with default parameters. Differentially expressed genes (DEGs) between two groups were obtained by implementing the FindMarkers function in Seurat with default methods and parameters.

*HybRISS (Hybridization-Based RNA In Situ Sequencing)*: Carotid artery tissue specimen was harvested during carotid endarterectomy in our clinical department for Vascular and Endovascular Surgery (Klinikum rechts der Isar, TUM) in Munich. Tissue was placed in RNAlater (Sigma-Aldrich, St. Louis, MO, USA) on ice until further processing. The tissue was cut in several pieces and the morphological most relevant pieces were snap frozen in liquid nitrogen and immediately embedded in Tissue-Tek O.C.T. (Optimal Cutting Temperature) Compound. OCT embedded tissues were stored at minus 80 °C until further use. Ten µm sections were cut with a cryotome and placed on SuperFrost Plus slides (Thermo Fisher Scientific, Waltham, MA, USA). Mounted slides were stored at -80 °C until the experiment was performed. Probe-design and the in situ sequencing was performed as described previously.[35,64]

*Statistical Analysis*: Differences in RNA expression, measured by qPCR, were calculated as fold change versus control using the mean ΔCt (defined as $Ct^{\text{target RNA}}$-$Ct^{\text{endogenous control}}$) within groups and compared using Student's *t* test. Two-tailed p-values were calculated. For differentially expressed gene analysis of the AoC experiments (shear stress vs null shear), a statistical threshold of p-value < 0.01 with fold change ≥ 2. Significant up- and down-regulated genes (at p-value < 0.01 and fold change ≥ 2) in the "Endothelial Cells (Flow vs Static)" comparison were mapped to 182 genes and assessed for KEGG pathway enrichment. For RNAseq of human carotid tissues a paired comparison between non-diseased (ctrl) and diseased (plaque) for each patient was performed (37 pairs in total). DEGs were determined using a statistical threshold corrected for multiple testing using the false discovery rate (FDR) adjustment (FDR-adjusted P < 0.05; fold change ≥ 2). For the analysis of transcriptomic changes between non-dilated and dilated samples from patients with AAA, a paired comparison was performed and a significant threshold of unadjusted p-value < 0.01 was applied. For silenced human carotid SMC, differential expression analysis of two conditions/groups was performed using the Ballgown R package and DEGs were calculated using FDR adjustment (FDR-adjusted P < 0.05) (Novogene, Cambridge, UK). Differential expression of genes was further analyzed through Gene Set Enrichment Analysis[65] using clusterProfiler R package together with Disease Ontology[66] and Molecular Signatures Database Hallmarks[67] gene sets.

## Supporting Information

Supporting Information is available from the Wiley Online Library or from the author.

## Acknowledgements

The authors acknowledge the support of Dr. Chika Okota and Prof. Mats Nilsson from the in situ sequencing facility at SciLife Lab (Stockholm, Sweden) for performing spatial transcriptomics on the human cohort of carotid plaques. This work was supported by funding from the Swedish Heart-Lung-Foundation (20210450), the Swedish Research Council (Vetenkapsrådet, 2019-01577), a DZHK Translational Research Project on microRNA modulation in aortic aneurysms, the CRC1123 and TRR267 of the German Research Council (DFG), the National Institutes of Health (NIH; 1R011HL150359-01), and the Bavarian State Ministry of Health and Care through the research project *DigiMed* Bayern.

Open access funding enabled and organized by Projekt DEAL.

## Conflict of Interest

We declare the following competing interest: Lars Maegdefessel is a scientific consultant and adviser for Novo Nordisk (Malov, Denmark), DrugFarm (Shanghai, China), and Angiolutions (Hannover, Germany), and received research funds from Roche Diagnostics (Rotkreuz, Switzerland).

## Author Contributions

Conceptualization: VP, LM; Methodology: VP, JP, NG, NH, FR, SM, EC, HJ; Investigation: VP, JP, GW, ZW, ZL; Visualization: NS, HHE, AB, ARB; Supervision: LM; Writing—original draft: VP, LM; Writing—review & editing: VP, LM, LB, RAB.

## Data Availability Statement

The data that support the findings of this study are available from the corresponding author upon reasonable request.

## Keywords

aortic aneurysms, arteries-on-a-chip, atherosclerosis, endothelial cells, smooth muscle cells, vascular diseases

Received: August 31, 2023
Revised: September 18, 2023
Published online:

[1] K. C. Aske, C. A. Waugh, *EMBO Rep.* **2017**, *18*, 1490.
[2] K. Ronaldson-Bouchard, G. Vunjak-Novakovic, *Cell Stem Cell* **2018**, *22*, 310.
[3] E. L. Jackson, H. Lu, *Integr. Biol. (Camb)*. **2016**, *8*, 672.
[4] S. N. Bhatia, D. E. Ingber, *Nat. Biotechnol.* **2014**, *32*, 760.
[5] P. Song, Z. Fang, H. Wang, Y. Cai, K. Rahimi, Y. Zhu, F. G. R. Fowkes, F. J. I. Fowkes, I. Rudan, *Lancet Global Health* **2020**, *8*, E721.
[6] S. S. Dhawan, R. P. Avati Nanjundappa, J. R. Branch, W. R. Taylor, A. A. Quyyumi, H. Jo, M. C. McDaniel, J. Suo, D. Giddens, H. Samady, *Expert Rev. Cardiovasc. Ther.* **2010**, *8*, 545.
[7] C. K. Zarins, D. P. Giddens, B. K. Bharadvaj, V. S. Sottiurai, R. F. Mabon, S. Glagov, *Circ. Res.* **1983**, *53*, 502.

[8] P. F. Davies, M. Civelek, Y. Fang, I. Fleming, *Cardiovasc. Res.* **2013**, *99*, 315.
[9] S. Aggarwal, A. Qamar, V. Sharma, A. Sharma, *Exp. Clin. Cardiol.* **2011**, *16*, 11.
[10] J. Golledge, *Nat. Rev. Cardiol.* **2019**, *16*, 225.
[11] A. J. Boyd, D. C. S. Kuhn, R. J. Lozowy, G. P. Kulbisky, *J. Vasc. Surg.* **2016**, *63*, 1613.
[12] I. O. Peshkova, G. Schaefer, E. K. Koltsova, *FEBS J.* **2016**, *283*, 1636.
[13] E. Cecchi, C. Giglioli, S. Valente, C. Lazzeri, G. F. Gensini, R. Abbate, L. Mannini, *Atherosclerosis* **2011**, *214*, 249.
[14] P. Libby, J. E. Buring, L. Badimon, G. K. Hansson, J. Deanfield, M. S. Bittencourt, L. Tokgözoğlu, E. F. Lewis, *Nat. Rev. Dis. Primers* **2019**, *5*, 56.
[15] G. L. Basatemur, H. F. Jørgensen, M. C. H. Clarke, M. R. Bennett, Z. Mallat, *Nat. Rev. Cardiol.* **2019**, *16*, 727.
[16] K. P. Dingemans, P. Teeling, J. H. Lagendijk, A. E. Becker, *Anat. Rec.* **2000**, *258*, 1.
[17] J. E. Wagenseil, R. P. Mecham, *Physiol. Rev.* **2009**, *89*, 957.
[18] Y. Fan, H. Lu, W. Liang, W. Hu, J. Zhang, Y. E. Chen, *J. Mol. Cell Biol.* **2017**, *9*, 352.
[19] J.-R. A. J. Moonen, et al., *KLF4 Recruits SWI/SNF to Increase Chromatin Accessibility and Reprogram the Endothelial Enhancer Landscape under Laminar Shear Stress*, **2020**, https://doi.org/10.1101/2020.07.10.195768.
[20] J.-F. Denis, M. R. Diagbouga, F. Molica, A. Hautefort, T. Linnerz, M. Watanabe, S. Lemeille, J. Y. Bertrand, B. R. Kwak, *Front. Physiol.* **2019**, *10*, 80.
[21] A. Barzegari, V. Gueguen, Y. Omidi, A. Ostadrahimi, M. Nouri, G. Pavon-Djavid, *J. Cell. Physiol.* **2020**, *235*, 5072.
[22] K.-C. Wang, Y.i-T. Yeh, P. Nguyen, E. Limqueco, J. Lopez, S. Thorossian, K.-L. Guan, Y.i-S. J. Li, S. Chien, *Proc. Natl. Acad. Sci. U. S. A.* **2016**, *113*, 11525.
[23] M. A. Marletta, *Trends Biochem. Sci.* **1989**, *14*, 488.
[24] D. Predescu, S. Predescu, J. Shimizu, K. Miyawaki-Shimizu, A. B. Malik, *Am. J. Physiol. Lung Cell. Mol. Physiol.* **2005**, *289*, L371.
[25] J. Pelisek, R. Hegenloh, S. Bauer, S. Metschl, J. Pauli, N. Glukha, A. Busch, B. Reutersberg, M. Kallmayer, M. Trenner, H. Wendorff, P. Tsantilas, S. Schmid, C. Knappich, C. Schaeffer, T. Stadlbauer, G. Biro, U. Wertern, F. Meisner, K. Stoklasa, A.-L. Menges, O. Radu, S. Dallmann-Sieber, A. Karlas, E. Knipfer, C. Reeps, A. Zimmermann, L. Maegdefessel, H.-H. Eckstein, *J. Clin. Med.* **2019**, *8*, 251.
[26] D. N. Ku, D. P. Giddens, C. K. Zarins, S. Glagov, *Arterioscler. Dallas Tex* **1985**, *5*, 293.
[27] Y. Takehara, et al., *Magn. Reson. Med.* **2020**, *19*, 235.
[28] R. Klemenz, E. Frohli, R. H. Steiger, R. Schafer, A. Aoyama, *Proc. Natl. Acad. Sci. U. S. A.* **1991**, *88*, 3652.
[29] A. J. Cocciolone, J. Z. Hawes, M. C. Staiculescu, E. O. Johnson, M. Murshed, J. E. Wagenseil, *Am. J. Physiol. Heart Circ. Physiol.* **2018**, *315*, H189.
[30] X. Wang, S. Abraham, J. A. G. McKenzie, N. Jeffs, M. Swire, V. B. Tripathi, U. F. O. Luhmann, C. A. K. Lange, Z. Zhai, H. M. Arthur, J. W. B. Bainbridge, S. E. Moss, J. Greenwood, *Nature* **2013**, *499*, 306.
[31] J. Zhang, L. Zhu, J. Fang, Z. Ge, X. Li, *J. Exp. Clin. Cancer Res.* **2016**, *35*, 29.
[32] K. T. Pang, C. W. Fhu, M. Ghim, H. M. Tay, H. W. Hou, Q. Lu, C. M. Warboys, X. Wang, P. D. Weinberg, *Atherosclerosis* **2018**, *275*, e37.
[33] K. T. Pang, M. Ghim, C. Liu, H. M. Tay, C. W. Fhu, R. N. Chia, B. Qiu, P. Sarathchandra, A. H. Chester, M. H. Yacoub, F. L. Wilkinson, R. Weston, C. M. Warboys, H. W. Hou, P. D. Weinberg, X. Wang, *Front. Cell Dev. Biol.* **2021**, *9*, 706143.
[34] F. Fasolo, G. Winski, Z. Li, Z. Wu, H. Winter, J. Ritzer, N. Glukha, J. Roy, R. Hultgren, J. Pauli, A. Busch, N. Sachs, C. Knappich, H.-H. Eckstein, R. A. Boon, V. Paloschi, L. Maegdefessel, *Mol. Ther. Nucleic Acids* **2023**, *33*, 848.
[35] H. Lee, S. M. Salas, D. Gyllborg, M. Nilsson, *Direct RNA targeted transcriptomic profiling in tissue using Hybridization-based RNA In Situ Sequencing (HybRISS)*, **2020**, https://doi.org/10.1101/2020.12.02.408781.
[36] J. F. Bentzon, F. Otsuka, R. Virmani, E. Falk, *Circ. Res.* **2014**, *114*, 1852.
[37] J. N. Redgrave, P. Gallagher, J. K. Lovett, P. M. Rothwell, *Stroke* **2008**, *39*, 1722.
[38] J. L. Harman, H. F. Jørgensen, *Br. J. Pharmacol.* **2019**, *176*, 3741.
[39] S. M. Eken, H. Jin, E. Chernogubova, Y. Li, N. Simon, C. Sun, G. Korzunowicz, A. Busch, A. Bäcklund, C. Österholm, A. Razuvaev, T. Renné, H. H. Eckstein, J. Pelisek, P. Eriksson, M. González Díez, L. Perisic Matic, I. N. Schellinger, U. Raaz, N. J. Leeper, G. K. Hansson, G. Paulsson-Berne, U. Hedin, L. Maegdefessel, *Circ. Res.* **2017**, *120*, 633.
[40] A. Busch, J. Pauli, G. Winski, S. Bleichert, E. Chernogubova, S. Metschl, H. Winter, M. Trenner, A. Wiegering, C. Otto, J. Fischer, J. Reiser, J. Werner, J. Roy, C. Brostjan, C. Knappich, H.-H. Eckstein, V. Paloschi, L. Maegdefessel, *JCI Insight* **2021**, *6*, e140364.
[41] P. Cheng, R. C. Wirka, L. Shoa Clarke, Q. Zhao, R. Kundu, T. Nguyen, S. Nair, D. Sharma, H.-J. Kim, H. Shi, T. Assimes, J. Brian Kim, A. Kundaje, T. Quertermous, *Circulation* **2022**, *145*, 469.
[42] I. Morianos, G. Papadopoulou, M. Semitekolou, G. Xanthou, *J. Autoimmun.* **2019**, *104*, 102314.
[43] G. Cao, C. D. O'Brien, Z. Zhou, S. M. Sanders, J. N. Greenbaum, A. Makrigiannakis, H. M. DeLisser, *Am. J. Physiol. Cell Physiol.* **2002**, *282*, C1181.
[44] J.-J. Chiu, P.-L. Lee, C.-N. Chen, C.-I. Lee, S.-F.u Chang, L.i-J. Chen, S.-C. Lien, Y.a-C. Ko, S. Usami, S. Chien, *Arterioscler. Thromb. Vasc. Biol.* **2004**, *24*, 73.
[45] N. Resnick, H. Yahav, A. Shay-Salit, M. Shushy, S. Schubert, L. C. M. Zilberman, E. Wofovitz, *Prog. Biophys. Mol. Biol.* **2003**, *81*, 177.
[46] T. G. Papaioannou, C. Stefanadis, *Hell. J. Cardiol. HJC Hell. Kardiologike Epitheorese* **2005**, *46*, 9.
[47] B. D. Gelfand, F. H. Epstein, B. R. Blackman, *J. Magn. Reson. Imaging* **2006**, *24*, 1386.
[48] K. S. Cunningham, A. I. Gotlieb, *Lab. Investig.* **2005**, *85*, 9.
[49] J.-J. Chiu, S. Chien, *Physiol. Rev.* **2011**, *91*, 327.
[50] Y. S. Chatzizisis, M. Jonas, A. U. Coskun, R. Beigel, B. V. Stone, C. Maynard, R. G. Gerrity, W. Daley, C. Rogers, E. R. Edelman, C. L. Feldman, P. H. Stone, *Circulation* **2008**, *117*, 993.
[51] J. N. Oshinski, D. N. Ku, S. Mukundan, F. Loth, R. I. Pettigrew, *J. Magn. Reson. Imaging* **1995**, *5*, 640.
[52] J. Oshinski, J. Curtin, F. Loth, *J. Cardiovasc. Magn. Reson.* **2006**, *8*, 717.
[53] H. Kaneda, T. Arao, K. Matsumoto, M. A. De Velasco, D. Tamura, K. Aomatsu, K. Kudo, K. Sakai, T. Nagai, Y. Fujita, K. Tanaka, K. Yanagihara, Y. Yamada, I. Okamoto, K. Nakagawa, K. Nishio, *Br. J. Cancer* **2011**, *105*, 1210.
[54] R. J. Dekker, S. van Soest, R. D. Fontijn, S. Salamanca, P. G. de Groot, E.d VanBavel, H. Pannekoek, A. J. G. Horrevoets, *Blood* **2002**, *100*, 1689.
[55] D. Jacko, et al., *J. Appl. Physiol.* **2019**, *126*, 1607.
[56] A. Rao, D. Barkley, G. S. França, I. Yanai, *Nature* **2021**, *596*, 211.
[57] R. Barrile, A. D. van der Meer, H. Park, J. P. Fraser, D. Simic, F. Teng, D. Conegliano, J. Nguyen, A. Jain, M. Zhou, K. Karalis, D. E. Ingber, G. A. Hamilton, M. A. Otieno, *Clin. Pharmacol. Ther.* **2018**, *104*, 1240.
[58] H. Yu, D. Kang, M. Whang, T. Kim, J. Kim, *Adv. Healthcare Mater.* **2021**, *10*, 2100508.
[59] J. Ribas, H. Sadeghi, A. Manbachi, J. Leijten, K. Brinegar, Y.u S. Zhang, L. Ferreira, A. Khademhosseini, *Appl. In Vitro Toxicol.* **2016**, *2*, 82.
[60] M. Abudupataer, S. Zhu, S. Yan, K. Xu, J. Zhang, S. Luo, W. Ma, M.d F. Alam, Y. Tang, H. Huang, N. Chen, L.i Wang, G. Yan, J. Li, H. Lai, C. Wang, K. Zhu, W. Zhang, *Elife* **2021**, *10*, e69310.
[61] M. Cho, J.-K. Park, *ACS Biomater. Sci. Eng.* **2020**, *6*, 5326.

[62] A. Günther, S. Yasotharan, A. Vagaon, C. Lochovsky, S. Pinto, J. Yang, C. Lau, J. Voigtlaender-Bolz, S.-S. Bolz, *Lab Chip* **2010**, *10*, 2341.
[63] V. Paloschi, M. Sabater-Lleal, H. Middelkamp, A. Vivas, S. Johansson, A. van der Meer, M. Tenje, L. Maegdefessel, *Cardiovasc. Res.* **2021**, *117*, 2742.
[64] D. Gyllborg, C. M. Langseth, X. Qian, E. Choi, S. M. Salas, M. M. Hilscher, E.d S. Lein, M. Nilsson, *Nucleic Acids Res.* **2020**, *48*, e112.
[65] A. Subramanian, P. Tamayo, V. K. Mootha, S. Mukherjee, B. L. Ebert, M. A. Gillette, A. Paulovich, S. L. Pomeroy, T. R. Golub, E. S. Lander, J. P. Mesirov, *Proc. Natl. Acad. Sci. U. S. A.* **2005**, *102*, 15545.
[66] L. M. Schriml, C. Arze, S. Nadendla, Y.-W. W. Chang, M. Mazaitis, V. Felix, G. Feng, W. A. Kibbe, *Nucleic Acids Res.* **2012**, *40*, D940.
[67] A. Liberzon, C. Birger, H. Thorvaldsdóttir, M. Ghandi, J. P. Mesirov, P. Tamayo, *Cell Syst.* **2015**, *1*, 417.